2

UCRL-ID-109921

Modeling Fluid-Rock Interaction at Yucca Mountain, Nevada: A Progress Report

B.E. Viani
C.J. Bruton

Publication Date: August 1992

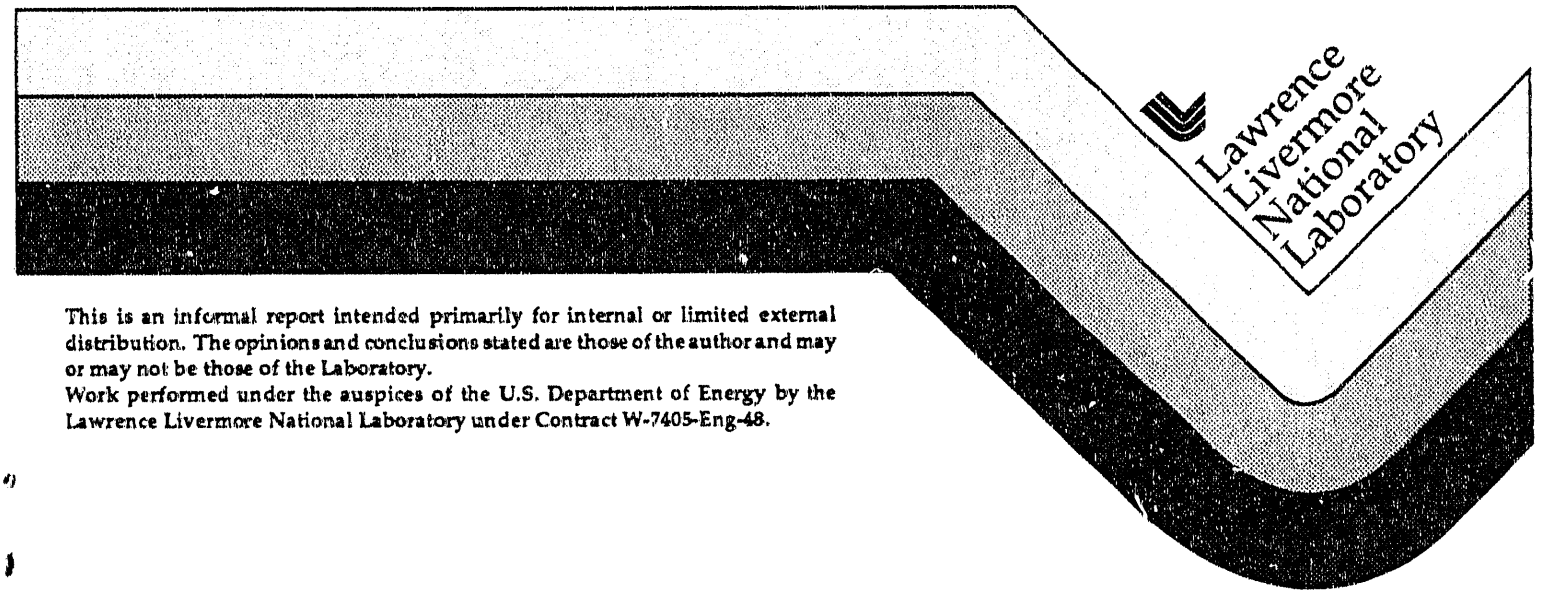

DISCLAIMER

Prepared by Yucca Mountain Site Characterization Project (YMP) participants as part of the Civilian Radioactive Waste Management Program. The YMP is managed by the Yucca Mountain Site Characterization Project Office of the U.S. Department of Energy, Las Vegas, Nevada.

UCRL-ID--109921

DE92 041080

Modeling Fluid-Rock Interaction at Yucca Mountain, Nevada: A Progress Report

Brian E. Viani and Carol J. Bruton

April 15, 1992

Abstract

Volcanic rocks at Yucca Mountain, Nevada are being assessed for their suitability as a potential repository for high-level nuclear waste. Recent progress in modeling fluid-rock interactions, in particular the mineralogical and chemical changes that may accompany waste disposal at Yucca Mountain, will be reviewed in this publication.

In Part I of this publication, "Geochemical Modeling of Clinoptilolite-Water Interactions", solid-solution and cation-exchange models for the zeolite clinoptilolite are developed and compared to experimental and field observations. At Yucca Mountain, clinoptilolite, which is found lining fractures and as a major component of zeolitized tuffs, is expected to play an important role in sequestering radionuclides that may escape from a potential nuclear waste repository.

The solid–solution and ion–exchange models were evaluated by comparing predicted stabilities and exchangeable cation distributions of clinoptilolites with: 1) published binary exchange data; 2) compositions of coexisting clinoptilolites and formation waters at Yucca Mountain; 3) experimental sorption isotherms of Cs and Sr on zeolitized tuff; and 4) high temperature experimental data. Good agreement was found between predictions and experimental data, especially for binary exchange and Cs and Sr sorption on clinoptilolite. However, additional model refinement is required to provide adequately for the preference of clinoptilolite exchange site(s) for K and to predict the energetic consequences of changes in the hydration state of clinoptilolite. In addition, there is a critical need for cation exchange data at elevated temperature.

Part II of this publication, "Geochemical Simulation of Fluid–Rock Interactions at Yucca Mountain", describes preliminary numerical simulations of fluid-rock interactions at Yucca Mountain. The solid-solution model developed in the first part of the paper is used to evaluate the stability and composition of clinoptilolite and other minerals in the host rock under ambient conditions and after waste emplacement.

Summary

Volcanic rocks at Yucca Mountain, Nevada are being assessed for their suitability as a potential repository for high-level nuclear waste. Recent progress in modeling fluid-rock interactions, in particular the mineralogical and chemical changes that may accompany waste disposal at Yucca Mountain, will be reviewed in this publication.

In Part I of this publication, "Geochemical Modeling of Clinoptilolite-Water Interactions", solid-solution and cation-exchange models for the zeolite clinoptilolite are developed and compared to experimental and field observation. At Yucca Mountain, clinoptilolite, which is found lining fractures and as a major component of zeolitized tuffs, is expected to play an important role in sequestering radionuclides that may escape from a potential nuclear waste repository. To fully simulate clinoptilolite-water interactions, the interrelated processes of dissolution/precipitation and ion-exchange were modeled. A solid-solution model was developed and implemented in geochemical modeling code package EQ3/6 to simulate instantaneous or kinetically controlled dissolution/precipitation of clinoptilolite. Cation-exchange models have been implemented to simulate ion exchange for cases in which clinoptilolite is not in overall equilibrium with the fluid phase and in which there is no change in the quantity of clinoptilolite in the system. Because the cation-exchange models can be applied independently of a specific solid phase, unlike solid-solution models, they can be used to simulate ion exchange in multi-phase exchangers such as soils, and exchangers for which thermodynamic stability data are not available.

Solid-solution model – Five steps were involved in the development of a solid-solution model describing compositional variation on the exchange site of clinoptilolite, and in the derivation of component end-member properties:

1) Thermodynamic data for a natural clinoptilolite were compiled from published calorimetric data and recalculated to be consistent with the EQ3/6 thermodynamic data base.
2) Free energies of cation exchange on clinoptilolite at 25 °C were compiled from reported binary exchange data.
3) A modified ideal site-mixing solid-solution model consistent with published cation-exchange data was defined. According to this model, the activity of the kth component end-member, a_k, is related to its mole fraction in the solid solution, X_k, according to

$$a_k = X_k^N ,$$

where N is the stoichiometry of the exchange site for homoionic components bearing monovalent cations.
4) Standard state chemical potentials of component end-members were calculated from the data and model obtained by steps 1–3.
5) Heat capacity power functions and molar third-law entropies of the component end-members were estimated using published algorithms.

Cation exchange models – The Vanselow and Gapon convention cation-exchange models were incorporated into EQ3/6. Ion exchange is assumed to be instantaneous. The Vanse-

low and Gapon models differ in the stoichiometry of the exchanger components used to write the exchange reaction. The component used to describe exchange according to the Vanselow model is M-Z_m, where M is a cation of valence m and Z represents one equivalent of exchanger. The component used to describe exchange according to the Gapon model is $M_{1/m}$-Z. We consider only ideal exchange; thus, for both models, the activity of an exchanger component can be equated to its mole fraction in the exchanger. Both the Vanselow and Gapon models are numerically indistinguishable for exchange involving only monovalent cations, but differ for all other exchanges. Both the Gapon and modified ideal site-mixing models, which are numerically equivalent, result in normalized binary isotherms that are independent of the presence of a third cation on the exchanger. In contrast, both the ideal site-mixing solid-solution model and the Vanselow exchange convention predict binary cation-exchange equilibria that are dependent on the concentration of other cations on the exchanger.

As a first approximation to the solid-solution and cation-exchange models, we have assumed that water of hydration in clinoptilolite does not play a role in the thermodynamics of the exchange reaction. This assumption is strictly valid only if each clinoptilolite end-member component has the same number of waters of hydration. We chose to assume that the numbers of waters of hydration are the same for each component and are equal to the number of waters measured by Johnson et al. (1991) for clinoptilolite equilibrated at a relative humidity of 50%.

Model evaluation – The solid-solution and ion-exchange models were evaluated by comparing predicted stabilities and exchangeable cation distributions of clinoptilolites with: 1) published binary exchange data; 2) compositions of coexisting clinoptilolites and formation waters at Yucca Mountain; 3) experimental sorption isotherms of Cs and Sr on zeolitized tuff; and 4) high temperature experimental data.

Published binary exchange data – The cation-exchange model based on the Gapon convention was combined with published exchange energies to calculate exchange isotherms for comparison with experimentally-derived isotherms. The isotherms defined by the experimental data points are reasonably matched by the predicted isotherms based on a single exchange site. However, a two-site Gapon model provided the best match between model and experiment. It appears that this modeling approach with either the one- or two-site cation-exchange models can reasonably describe available experimental data for clinoptilolite.

Compositions of coexisting clinoptilolites and formation waters – Chemical analyses of waters sampled from wells penetrating the saturated zone at Yucca Mountain, Nevada were used to predict the exchangeable cation distribution of clinoptilolites in equilibrium with the waters. The compositions predicted using the one-site Gapon model were compared to measured clinoptilolite compositions from Yucca Mountain. Predicted compositions of clinoptilolite approximately span the range of observed Na–Ca ratios. However, natural clinoptilolites are significantly enriched in K relative to predicted compositions. It is possible that chemistries of sampled waters do not accurately reflect small-scale variations in in-situ fluid chemistries. In addition, we cannot be sure that the sampled fluids were actually in contact with the clinoptilolites for which compositional data is available. Further

refinement of the models is required to provide adequately for the preference of clinoptilolites exchange site(s) for K.

Sorption of Cs and Sr on tuff – Experimental measurement of the partition coefficients, K_d, and sorption isotherms of Cs and Sr from J–13 groundwater onto crushed tuff from Yucca Mountain were compared with K_d's and isotherms predicted using a one-site Vanselow cation-exchange model. There is good agreement between model prediction and measurement for Sr sorption over a wide range in K_d values. For Cs, the model underestimates K_d's for most of the smectite-rich samples and for samples with low cation exchange capacities. The underestimation of Cs K_d's for the smectite-rich samples may arise because the exchange energies used in the modeling represent the overall energies of exchange and do not reflect the high affinity that some sites have for Cs. In contrast, predicted adsorption isotherms agree closely with the measured isotherms for both Cs and Sr on a clinoptilolite-rich tuff sample. This agreement suggests that adsorption of trace quantities of Cs and Sr at 25 °C can be adequately modeled using a simple one-site model. It is apparent that the equilibrium exchange model we have implemented can serve to integrate the mineralogical, solution, and sorption data to a degree impossible using empirical isotherms and/or statistical approaches. The generally good agreement between model predictions and sorption measurements means that the significant mineralogical data collected by Los Alamos National Laboratory can be utilized to predict Cs and Sr K_d's for tuffs for which sorption data is lacking.

Exchange at high temperature – Few reliable data exist to test predictions of clinoptilolite exchange site distributions at elevated temperature. Calculations of the relation between the Ca content of clinoptilolite and the Ca concentration in solution using a one-site Gapon model are in accord with high-temperature, experimentally observed water and clinoptilolite compositions. Binary exchange isotherms computed using estimates of high temperature exchange energies predict that the preference of clinoptilolite for Ca vs. Na, K, and Cs increases with increasing temperature. Increasing temperatures at Yucca Mountain would, therefore, favor the stability of Ca-rich clinoptilolites relative to Na-rich clinoptilolites. Accordingly, Ca will tend to replace Na on the exchange site as temperatures increase. Increasing ionic strength at 25 °C from 0.001 N to 1.0 N favors Na and K rather than Ca in the exchange site. The preference of clinoptilolite for Na and K at increased ionic strength would thus be opposed to its preference for Ca at increased temperature.

Part II of this publication, "Geochemical Simulation of Fluid–Rock Interactions at Yucca Mountain", describes preliminary numerical simulations of fluid-rock interactions at Yucca Mountain. The solid-solution model developed in the first part of the paper is used to evaluate the stability and composition of clinoptilolite and other minerals in the host rock under ambient conditions and after waste emplacement.

Controls of mineral evolution at Yucca Mountain – The stability of host rock minerals and the potential for mineralogical reactions will be influenced by changes in temperature that occur when waste packages are emplaced in the repository. The thermal response of clinoptilolite is of particular interest because of its potential impact on the permeability of clinoptilolite-rich zones, and on the cation exchange capacity and composition of clino-

ptilolite. Kerrisk (1983) and Duffy (1984) postulated that the identity of the silica polymorph and the corresponding activity of aqueous silica control the observed mineralogical zones at Yucca Mountain. Diagenetic reactions in Yucca Mountain volcanic rocks with depth were simulated using EQ3/6 to evaluate the relationship between the identity of the silica polymorph and the diagenetic assemblage. In this study, the overall stability of the clinoptilolite solid solution was evaluated at the same time as the exchange cation occupancies were computed as a function of both temperature and the identity of co-precipitates.

Despite the fact that the kinetics of transformation of the silica polymorphs were not included explicitly in the simulations, the predicted diagenetic sequence agrees favorably with observed diagenetic zones I, II, III and IV at Yucca Mountain (Broxton, Bish and Warren, 1987). The correspondence between observed and predicted mineralogical assemblages supports the contention that the identity of the silica polymorph and the corresponding activity of aqueous silica control diagenetic evolution at Yucca Mountain. Predicted compositional trends of clinoptilolite also agree well with observed trends with depth of exchangeable cations in clinoptilolite-group minerals from diagenetic zones II and III at Yucca Mountain.

Potential impact of fluid–rock interactions at elevated temperature – Geochemical simulations of reaction between J–13 water and Topopah Spring tuff suggest that a zeolite–cristobalite–dioctahedral smectite secondary mineral assemblage, consistent with mineralogy in diagenetic zones I and II at Yucca Mountain, is the most likely phase assemblage in metastable equilibrium with J–13 water at 25°C. Simulations indicate that increasing temperature will tend to favor the stability of minerals that are already abundant at Yucca Mountain.

Calculations suggest that the impact of observed variations of pH (7 to 10) and Eh (–0.2 to 0.8 volts) of J–13 water on diagenetic mineralogy will be greatest during the early stages of reaction. The impact will be minimized as the rock and fluid continue to react and as the rock:fluid ratio increases. Eh, as expected, affects the identity of the Fe–bearing precipitate, whereas the impact of changes in the initial pH is minimal.

Table of Contents

Abstract i

Summary iii

List of Tables ix

List of Figures x

Introduction 1

I. Geochemical Modeling of Clinoptilolite-Water Interactions 2

Development of Cation-Exchange and Solid-Solution Models for Clinoptilolite 3

Summary of modeling approaches 3
Solid-solution model development 4
Cation-exchange model development 8
Implications of models: Exchanger selectivity and binary exchange isotherms 10
Water of hydration and thermodynamic properties of clinoptilolite 12

Model Validation 13

Binary exchange in clinoptilolite 13
Correlations between clinoptilolite composition and formation water chemistry at Yucca Mountain 15
Partition coefficients and sorption isotherms for Cs and Sr on Yucca Mountain tuff samples 20
Clinoptilolites in high temperature experiments 25

Effects of Temperature and Ionic Strength on Exchangeable Cation Distribution 29

Future Work 29

II. Geochemical Simulation of Fluid–Rock Interactions at Yucca Mountain 31

Introduction 32

Controls of Mineral Evolution at Yucca Mountain 32

Potential Impact of Fluid–Rock Interactions at Elevated Temperature 35

Equilibrium between Yucca Mountain waters and subsurface mineralogy 35
Effect of temperature on interactions between J–13 water and Topopah Spring tuff 36
Effect of initial Eh and pH of J–13 water on mineralogic reactions 39

References 43

Appendix A. Derivation of Modified Ideal Site-Mixing Solid-Solution Model . 48

Appendix B. Implementation in EQ3/6 – Solid-Solution Model 52

Appendix C. Estimation of Entropy and Heat Capacity Power Function Coefficients 53

Appendix D. Implementation in EQ3/6 – Cation-Exchange Models 55

Appendix E. Thermochemical Data for Clinoptilolite 58

List of Tables

Table 1. Thermodynamic data for a natural clinoptilolite and component homoionic end-members of a clinoptilolite solid solution referenced to α–quartz. 5

Table 2. Heat capacity power function coefficients and temperature limits of applicability for a natural clinoptilolite and component end-members of a clinoptilolite solid solution. 5

Table 3. Exchange energies used to calculate the free energies of clinoptilolite component end-members. 6

Table 4. Parameters used in two–site exchange model. 15

Table 5. Parameters used to model sorption of Cs and Sr on Yucca Mt. tuffs using EQ3/6: Example using sample YM–38. 22

Table A.1. Site–mixing parameters for coupled cation–vacancies describing Gapon and Vanselow exchange models. 51

Table E.1. Thermodynamic properties of selected zeolites in EQ3/6 data base data0.com.R7. 59

Table E.2. Heat capacity power function coefficients and temperature limits of applicability for selected zeolites in EQ3/6 data base data0.com.R7 . 60

List Of Figures

Figure 1. Normalized non-preference Na-Ca binary isotherms for Vanselow, Gapon, ideal site-mixing, and modified ideal site-mixing models at 1.0 and 0.001 N. 11

Figure 2. Binary exchange data from Ames (1964a,b) in 1 N solution at 25 °C compared to exchange isotherms predicted using the one- and two-site Gapon convention models. 14

Figure 3. Predicted exchange isotherms at 25 °C for Na-Ca exchange at a total normality of Na plus Ca in J-13 water of 0.00253 and K-Ca exchange at a total normality of K plus Ca in J-13 water of 0.000755. 16

Figure 4. Comparison between predicted and analytical compositions of clinoptilolites at Yucca Mountain for wells UE25 b-1, UE25 P-1, J-13 and USW H-4. 18

Figure 5. Ternary plot comparing analyzed exchangeable cation distributions of clinoptilolites from the saturated zone at Yucca Mountain with predicted clinoptilolite compositions. 20

Figure 6. Predicted vs. experimental partition coefficients for Cs and Sr on samples of Yucca Mountain tuff. 23

Figure 7. Predicted and experimental isotherms for Cs and Sr on sample YM-38 from the Bedded Tuff of Calico Hills, Yucca Mountain. 24

Figure 8. Effect of clinoptilolite composition and abundance on predicted values of the partition coefficient of Cs in a clinoptilolite-bearing sample. 26

Figure 9. Relation between equivalent percent of Ca on the exchange site of clinoptilolite and the concentration of Ca in solution at 250 °C. 27

Figure 10. Relation between temperature and Cs Kd predicted using the one-site Vanselow model for sample YM-38 from the Bedded Tuff of Calico Hills in contact with J-13 groundwater. 28

Figure 11. Predicted adsorption isotherms for Na-Ca exchange on clinoptilolite assuming a one-site Gapon model for 0.001 and 1.0 N solutions at 25 and 100 °C and for 0.001 to 1.0 N solutions at 25 °C. 30

Figure 12. Simulation results for reaction of Topopah Spring glass shards with J-13 water from 25 to 90 °C. 34

Figure 13. Predicted paragenetic sequence for reaction of Topopah Spring tuff with J-13 water from 25 to 90 °C. 37

Figure 14. Ranges in Eh and pH measured in Yucca Mountain waters from the saturated zone. 40

Figure 15. Predicted paragenetic sequences for reaction of Topopah Spring tuff with J-13 water at 90 °C assuming initial J-13 waters with a pH = 7 and Eh of 0.8 and -0.2 volts; and pH = 10 and Eh of 0.63 and -0.2 volts. 42

Figure E.1. Activity diagram for the system Na–K–Ca–Al–Si–H_2O at 25 °C depicting mineral stability as a function of the logarithm of the activity of aqueous silica in solution and the logarithm of the ratio of the activity of the Ca^{2+} ion to the square of the activity of H^+ ion in solution. 61

Introduction

Volcanic rocks at Yucca Mountain, Nevada are being assessed for their suitability as a potential repository for high-level nuclear waste. Burial of nuclear waste will heat the volcanic host rocks and provide an impetus for fluid flow in both the unsaturated and saturated zones. The goal of our studies is to determine the mineralogical and chemical changes that may accompany waste disposal. Recent progress in modeling fluid-rock interactions at Yucca Mountain will be reviewed in this publication. For additional information regarding the Yucca Mountain site, see Glassley (1986).

Part I of this publication, "Geochemical Modeling of Clinoptilolite-Water Interactions", describes the development and testing of solid-solution and cation-exchange models for clinoptilolite. At Yucca Mountain, clinoptilolite–rich formations and clinoptilolite–lined fractures are expected to play an important role in sequestering radionuclides that may escape from a potential nuclear waste repository. The stability of clinoptilolite with respect to temperature is also under question. Geochemical modeling codes will be used to predict the stability of clinoptilolite under anticipated repository conditions and to predict the potential for alteration of the sorptive properties of clinoptilolite-rich zones. Because the composition of clinoptilolite is variable, solid-solution and cation–exchange models were incorporated into the modeling code package EQ3/6 (Wolery, 1983; Wolery et al., 1990) in order to address the above issues.

Part II of this publication, "Geochemical Simulation of Fluid–Rock Interactions at Yucca Mountain", describes preliminary numerical simulations of fluid-rock interactions at Yucca Mountain. The solid-solution model developed in the first part of the paper is used to evaluate the stability and composition of clinoptilolite and other minerals in the host rock under ambient conditions and after waste emplacement.

The simulations, through simultaneous consideration of all potential fluid–mineral reactions, illustrate the dependence of the composition and sorptive properties of clinoptilolite and other phases on the many reactions which are occurring simultaneously at any given point in time. Identification of mineral precipitation and dissolution events that result from waste disposal allows potential changes in the transport properties of the volcanic tuffs, required by hydrologic models, to be evaluated. In addition, the role of clinoptilolite as a sorptive barrier can be more fully evaluated in terms of the overall chemical evolution of the system.

I. Geochemical Modeling of Clinoptilolite-Water Interactions

Development of Cation-Exchange and Solid-Solution Models for Clinoptilolite

Summary of modeling approaches

To fully simulate clinoptilolite-water interactions, the interrelated processes of *dissolution/precipitation* and *ion-exchange* must be modeled. A *solid-solution model* has been developed and implemented in EQ3/6 (Bourcier, 1985; Wolery, 1983; Wolery et al., 1990) to predict the composition of solid solutions. The solid-solution models are linked to precipitation/dissolution models which allow the mass of a solid solution to vary as it changes composition during solid-fluid interaction. *Cation-exchange models* have been implemented in EQ3/6 to predict cation distribution on exchange sites assuming that the mass of the exchanger, for example, a non-reactive framework or surface, is invariant during solid-fluid interaction.

Solid-solution model – A solid-solution model (modified ideal site–mixing) describing the mixing of component clinoptilolite end-members was developed to predict clinoptilolite stability and to predict equilibrium phase relationships between clinoptilolite and associated phases as a function of total system composition, aqueous fluid composition, and temperature. Using this approach, the composition of a clinoptilolite solid solution in contact with an aqueous fluid can be predicted. As currently implemented, the solid-solution model for clinoptilolite only accounts for compositional variability on the exchange site(s). Extension of the model to account for compositional variability on structural sites will require additional compositional and thermochemical data.

Cation-exchange model – In order to model the sorptive potential of clinoptilolite it is necessary to predict the composition of the clinoptilolite *exchange site(s)* as a function of solution composition, mass of clinoptilolite and solution, and temperature. Two *cation-exchange models* (Gapon and Vanselow) describing the mixing of cations on exchange sites were implemented in EQ3/6. Decoupling ion exchange from dissolution/precipitation was effected by treating the exchanger as if it were a *fictive aqueous ligand*, thereby avoiding association of exchangers with specific solid phases, and preventing equilibrium between the exchanger ligand and any component save the exchange cations. The exchange models were incorporated in a manner that allows simulation of ion exchange on exchangers having *multiple independent* exchange sites.

Comparison of modeling approaches – Although the solid-solution and cation-exchange models both address compositional variability of the exchange site, they differ in the chemical processes they simulate. The cation-exchange model can be used to simulate ion-exchange for cases in which clinoptilolite is *not in overall equilibrium* with the fluid phase and there is no change in the quantity of clinoptilolite in the system. The solid-solution model simulates instantaneous or kinetically controlled dissolution/precipitation of clinoptilolite. Because the cation-exchange models can be applied independently of a specific solid phase, unlike solid-solution models, they can be used to simulate ion exchange in multi-phase exchangers such as soils, and exchangers for which thermodynamic stability data are not available. However, cation-exchange models cannot be used for simulations

in which the exchanger phase is created or destroyed because the exchanger phase is treated as a fictive aqueous ligand which, by definition, cannot undergo any reaction with components other than the exchange cations and hence, cannot be made or destroyed.

Because the form of a solid-solution model in effect defines an exchange model, it is convenient to incorporate solid-solution and cation-exchange models that are numerically equivalent so that simulations can be made using both models. The modified ideal site-mixing model (described below) is numerically equivalent to the Gapon exchange model. A present, there is no solid-solution model that is numerically equivalent to the Vanselow exchange model. The development of the solid-solution and exchange models follow.

Solid-solution model development

To describe the thermodynamic properties of a solid-solution, the thermodynamic properties of the component end-members must be known as a function of temperature and pressure. In addition, the relationship between the activity and concentration of an end-member component in the solid-solution must be described. Because only compositional variation on the exchange site is considered, the homoionic exchange forms of clinoptilolite correspond to the component end-members of the clinoptilolite solid solution. Lacking thermodynamic data for homoionic component end-members of clinoptilolite, we derived this data from thermochemical data reported for a natural clinoptilolite. Five steps were involved in the development of the solid-solution model and in the derivation of end-member properties:

1) Thermodynamic data for a natural clinoptilolite were compiled.
2) Free energies of cation exchange on clinoptilolite at 25 °C were compiled.
3) A solid-solution model consistent with published cation-exchange data was defined.
4) Standard state chemical potentials of component end-members were calculated from information obtained in steps 1–3.
5) Heat capacity functions and entropies of the component end-members were estimated using published algorithms.

Descriptions of these steps follow.

Thermodynamic data for a natural clinoptilolite – Thermochemical data for a (Na, K, Ca, Mg, Sr, Ba, Mn)–clinoptilolite has been reported by Johnson et al. (1991). This data, derived from calorimetric measurements referenced to the heat of dissolution of silicalite, was recalculated in order to be referenced to α-quartz (see Appendix E) to insure consistency with GEMBOCHS, the thermodynamic data base used at LLNL (Delany and Lundeen, 1991) (Tables 1 and 2).

Free energies of cation exchange at 25°C – Binary cation-exchange isotherms have been experimentally determined for various clinoptilolites at temperatures ranging from ambient to 75°C (Ames, 1964a, 1964b; Barrer et al., 1967; Frysinger, 1962; Howery and Thomas, 1965; Hulbert, 1987). The free energies of exchange derived from isotherms measured at 25 and 30°C for clinoptilolites from Washington, Oregon, and California are similar. These data were used to develop a self-consistent set of exchange energies (Table 3).

Table 1. Thermodynamic data for a natural clinoptilolite[1] and component homoionic end-members of a clinoptilolite solid solution referenced to α–quartz (see text).

	$\Delta G^\circ_{f,298}$ kcal/mol	$S^\circ_{298} - S^\circ_0$ [2] cal/mol-K	V° cm^3/mol
Clinoptilolite	–4546.175	354.46	632.05
Clinoptilolite – Na[3]	–4535.926	360.22	632.05
Clinoptilolite – K	–4558.181	360.73	632.05
Clinoptilolite – Cs	–4568.686	373.13	632.05
Clinoptilolite – NH_4	–4389.269	----	----
Clinoptilolite – Ca	–4547.780	349.60	632.05
Clinoptilolite – Sr	–4552.547	353.78	632.05

(1) $(Sr_{0.036}Mg_{0.124}Ca_{0.761}Mn_{0.002}Ba_{0.062}K_{0.543}Na_{0.954})Al_{3.45}Fe_{0.017}Si_{14.533}O_{36} \cdot 10.922H_2O$; from Johnson et al. (1991).
(2) Because the entropy at 0 K is unknown, the difference between the entropy at 298 and that at 0 K is tabulated.
(3) Clinoptilolite–M refers to a clinoptilolite end-member with composition $M_\gamma(Al_{3.45}Fe_{0.017}Si_{14.533}O_{36}) \cdot 10.922H_2O$, where M is a cation with the γth stoichiometry such that M_γ totals 3.467 equivalents.

Table 2. Heat capacity power function coefficients and temperature limits of applicability for a natural clinoptilolite[1] and component end-members of a clinoptilolite solid solution.

	C_p power function coefficients[3]				C_p limit
	a	b	c	d	K
Clinoptilolite	11.987	----	1.5212	1.1032×10^{-3}	500
Clinoptilolite – Na[2]	18.552	–190020	1.5237	1.1032×10^{-3}	500
Clinoptilolite – K	19.003	158413	1.5303	1.1032×10^{-3}	500
Clinoptilolite – Cs	14.271	310961	1.5291	1.1032×10^{-3}	350
Clinoptilolite – NH_4	----	----	----	----	----
Clinoptilolite – Ca	7.146	40535	1.5171	1.1032×10^{-3}	500
Clinoptilolite – Sr	8.307	–2802.5	1.5172	1.1032×10^{-3}	500

(1,2) See footnotes to Table 1.
(3) C_p (cal/mol-K) = $a + bT^{-2} + cT + dT^2$

In order to derive component end-member properties from the data reported by Johnson et al. (1991), exchange energies for all cations occupying the exchange site are required. Free energies of exchange involving Mg, Ba, and Mn are not available. The assumption was made that the Mg and Mn exchange energies are equal to that for Ca, and that the energy of exchange of Ba is equal to Sr.

Table 3. Exchange energies used to calculate the free energies of clinoptilolite component end-members.

Exchange reaction (1)	Exchange energy, kcal/equiv (2)
Na —> K	-1.50
Na —> Cs	-2.33
Na —> ½ Mg	0.05 (3)
Na —> ½ Ca	0.05
Na —> ½ Sr	-0.05
Na —> ½ Ba	-0.05 (3)
Na —> ½ Mn	0.05 (3)

(1) Na —> K symbolizes the exchange reaction: Na-clinoptilolite + K^+ = K-clinoptilolite + Na^+
(2) Consistent set of exchange energies was compiled from Ames, 1964a,b; Barrer et al., 1967; Frysinger, 1962; and Howery and Thomas, 1965.
(3) Exchange energies for Mg, Ba, and Mn are not available. These listed values were assumed for the computation of the Na, K, Cs, Ca, and Sr end-member free energies but were not used to obtain data for Mg, Ba, and Mn end-members.

Solid–solution model: Modified ideal site–mixing model – For a solid solution composed of n components

$$G_{ss} = \sum_{k=1}^{n} X_k \mu_k^\circ + RT \sum_{k=1}^{n} X_k \ln a_k \quad , \qquad (1)$$

where G_{ss} is the molar free energy of a solid solution of a *specific composition* (e.g., the free energy of clinoptilolite measured by Johnson et al. (1991)), a_k, X_k, and μ_k° are the activity, mole fraction, and standard state chemical potential of the kth end-member component in the solid solution, respectively, R is the gas constant, and T is the temperature in kelvins (e.g., Wood and Fraser, 1977).

The relationship between the activity of a component, a_k, and its concentration in the solid solution, X_k, is defined by the model chosen to describe the mixing of components. We

have used a *modified ideal site–mixing model* to describe the activity-composition relationship; that is,

$$a_k = X_k^N \quad , \tag{2}$$

where N is the number of energetically equivalent positions in the site on which mixing of cations can occur. For solid solutions in which mixing occurs on a single site and in which all component end-members contain N cations on this site, Eq. (2) describes ideal mixing of components (Wood and Fraser, 1977). For the clinoptilolite solid solution, we equate N to the stoichiometry of the exchange site for homoionic components bearing monovalent cations. This is equal to the negative charge on the framework developed by isomorphous substitution of Al and Fe for Si. Derivation of this equation and its relationship to solid-solution models based on the ideal mixing of components and ideal mixing of cations on sites (ideal site–mixing) is given in Appendix A.

This model was chosen because it can reasonably match the limited cation exchange data available, it is numerically equivalent to a commonly applied cation-exchange convention (the Gapon model), and it is ideal; that is, it predicts that the mixing between any two components is unaffected by the presence of any other component. Implementation of the model into EQ3/6 followed the method outlined by Bourcier (1985) (see Appendix B).

Calculation of standard state chemical potentials of components – The standard state chemical potentials of the components, μ_k°, were calculated using the measured molar free energy of formation of the clinoptilolite solid solution, G_{ss}, the free energies of exchange, G^{exc}, and the modified ideal site-mixing model. For an n-component solid solution there are $n-1$ independent equilibrium exchange reactions of the form

$$(M_1)_{\nu_1}\text{–clinoptilolite} + \nu_k M_k = (M_k)_{\nu_k}\text{–clinoptilolite} + \nu_1 M_1 + \nu_{w_{1,k}}\mathrm{H_2O} \tag{3}$$

for $k = 2,n$. M_1 and M_k represent cations 1 and k, respectively, ν_1 and ν_k are their stoichiometries on the exchange site, and $\nu_{w1,k}$ is the difference in waters of hydration between the two end-members. Thus, $n-1$ equations

$$\begin{aligned}
G_{1,2}^{exc} &= \mu_2^\circ - \mu_1^\circ + \nu_1 \Delta G_{f,M_1}^\circ - \nu_2 \Delta G_{f,M_2}^\circ + \nu_{w_{1,2}} \Delta G_{f,H_2O}^\circ \ , \\
&\vdots \\
G_{1,k}^{exc} &= \mu_k^\circ - \mu_1^\circ + \nu_1 \Delta G_{f,M_1}^\circ - \nu_k \Delta G_{f,M_k}^\circ + \nu_{w_{1,k}} \Delta G_{f,H_2O}^\circ \ , \\
&\vdots \\
G_{1,n}^{exc} &= \mu_n^\circ - \mu_1^\circ + \nu_1 \Delta G_{f,M_1}^\circ - \nu_n \Delta G_{f,M_n}^\circ + \nu_{w_{1,n}} \Delta G_{f,H_2O}^\circ
\end{aligned} \tag{4}$$

follow from the equilibrium exchange reactions. $G^{exc}_{1,k}$ is the free energy of reaction for the conversion of compon nt 1 to component k, $\Delta G^{\circ}_{f,M_k}$ is the standard free energy of formation of cation M_k, and $\Delta G^{\circ}_{f,H_2O}$ is the standard free energy of formation of water. Equations (1) and (4) constitute a set of n equations in which all but the n μ°_k's are known. Using the molar free energy of formation for clinoptilolite from Table 1, the exchange energies from Table 3, and the standard free energies of formation of the cations and water from GEMBOCHS, the set of equations was solved for the μ°_k's (Table 1). NOTE: *The μ°_k values listed in* Table 1 *are specific to the particular solid-solution model we have chosen. A different set of values would have resulted had an alternative solid-solution model been used.*

Estimation of end-member entropies and heat capacity power functions – The molar third-law entropies and heat capacity power function coefficients were estimated for component end-members of the clinoptilolite solid-solution (Table 2) using the algorithms presented by Helgeson et al. (1978). The algorithms utilize solid–solid reference reactions written between the phase of interest and a structurally similar phase whose thermodynamic properties are known. Reference exchange reactions were written between the end-member of interest and the mixed-composition clinoptilolite studied by Johnson et al. (1991), using oxides to balance the reaction stoichiometry. The estimation was made assuming that all $\nu_{w1,k}$ were equal to *zero*; that is, the water of hydration for each end-member was the same (see below). Details of the estimation procedure are described in Appendix C.

Cation-exchange model development

Two cation-exchange models, Vanselow and Gapon, were incorporated into EQ3/6. For each model, the exchanger is treated as an aqueous ligand; thus, only instantaneous ion exchange is considered. Unlike the solid-solution model, the quantity of exchanger is constrained to be invariant during a simulation. This constraint arises because in order to implement these models in EQ3/6, it is necessary to define the exchanger ligand as a unique element. Appendix D describes the implementation of the cation exchange models in EQ3/6.

The Vanselow and Gapon models differ in the *stoichiometry* of the *exchanger components* used to write the exchange reaction. We consider only ideal exchange; thus, for *both* models, the activity of an exchanger *component* can be equated to its *mole fraction* in the exchanger. Both the Vanselow and Gapon models are numerically indistinguishable for exchange involving only monovalent cations, but differ for all other exchanges.

Vanselow exchange model – The component used to describe exchange according to the Vanselow model is M-Z_m, where M is a cation of valence m and Z represents one equivalent of exchanger. For heterovalent exchange (e.g., the exchange of Na by Ca) involving z equivalents of exchanger, the Vanselow model is described by the following exchange reaction

$$z\text{Na–}Z + z/2\ \text{Ca}^{++} = z/2\ \text{Ca–}Z_2 + z\text{Na}^{+} \quad . \tag{5}$$

The corresponding mass-action equation is

$$K = \frac{a_{\text{Ca–}Z_2}^{z/2}\ a_{\text{Na}^+}^{z}}{a_{\text{Na–}Z}^{z}\ a_{\text{Ca}^{++}}^{z/2}} \quad , \tag{6}$$

where a_{Na-Z} is the activity of the *Na–Z* exchange component, a_{Na+} is the activity of the Na^+ cation in solution, and K is the equilibrium constant for the exchange reaction. For ideal exchange, the activity of the exchange component is equal to

$$a_{M-Z_m} \equiv X_{M-Z_m} = x_M \quad , \tag{7}$$

where X_{M-Zm} is the mole fraction of *component* $M–Z_m$ in the exchanger and x_M is the mole fraction of *cation M* on the exchange site. *Thus, the activity of the exchange component in the ideal Vanselow model is equal to the mole fraction of the cation on the exchange site.* Considering one equivalent of exchanger, the equilibrium constant for ideal exchange according to the Vanselow convention, K_V, is

$$K_V = \frac{x_{\text{Ca}}^{1/2}\ a_{\text{Na}^+}}{x_{\text{Na}}\ a_{\text{Ca}^{++}}^{1/2}} \quad . \tag{8}$$

Gapon exchange model – The component used to describe exchange according to the Gapon model is $M_{1/m}$-Z. For heterovalent exchange involving z equivalents of exchanger, the Gapon model is described by the exchange reaction

$$z\text{Na–}Z + z/2\ \text{Ca}^{++} = z\text{Ca}_{1/2}\text{–}Z + z\text{Na}^{+} \tag{9}$$

and corresponding mass action equation

$$K = \frac{a_{\text{Ca}_{1/2}\text{–}Z}^{z}\ a_{\text{Na}^+}^{z}}{a_{\text{Na–}Z}^{z}\ a_{\text{Ca}^{++}}^{z/2}} \quad . \tag{10}$$

For ideal exchange, the activity of the exchange component is equal to

$$a_{M_{1/m}-Z} \equiv X_{M_{1/m}-Z} = E_M \quad , \tag{11}$$

where $X_{M_{1/m}-Z}$ is the mole fraction of *component* $M_{1/m}$–Z in the exchanger and E_M is the *equivalent fraction of cation M* on the exchange site. *Thus, the activity of the exchange component in the ideal Gapon model is equal to the equivalent fraction of the cation on the exchange site.* For one equivalent of exchanger, the equilibrium constant for ideal exchange according to the Gapon convention, K_G, is

$$K_G = \frac{E_{Ca}\ a_{Na^+}}{E_{Na}\ a^{1/2}_{Ca^{++}}} \quad . \tag{12}$$

Implications of models: Exchanger selectivity and binary exchange isotherms

Exchanger selectivity: Separation factor – A binary exchange isotherm describes the relationship between the normalized equivalent fraction of a cation in the exchanger (the equivalent fraction based only on the cations comprising the binary pair) and its normalized equivalent fraction in solution. The selectivity of the exchanger for a cation can be quantified in terms of a *separation factor* that describes the relative distribution of the exchange cations between solution and exchanger. For binary exchange between cations 1 and 2 the separation factor, S, for cation 1 is

$$S_1 = \frac{\overline{E}_1\ E_2}{\overline{E}_2\ E_1} \quad , \tag{13}$$

where $\overline{E}_1$ and E_1 are the equivalent fractions of cation 1 on the exchanger and in solution, respectively. It is important to note that for a given binary, the selectivity of the exchanger for a cation often varies with composition. Consequently, care must be taken when comparing the selectivity of an exchanger for various cations to insure that it is done at an equivalent level of a common cation. An alternative method of comparing the affinity of an exchanger for a series of cations is to use the *energy* of exchange relative to a common ion.

Comparison of binary exchange isotherms predicted from the different models – Differences between the various solid-solution and cation-exchange models can be examined by comparing the binary exchange isotherms predicted by each model (Figure 1a,b). Normalized non-preference (K= 1) binary isotherms have been computed for Na–Ca exchange according to the Gapon and Vanselow exchange conventions, and for ideal site-mixing and modified ideal site–mixing solid-solution models. Isotherms are shown for binary exchange in the absence of any other cation (Figure 1a), and for exchange in the presence of a constant equivalent fraction (0.95, Figure 1b) of a second divalent cation (M^{++}). The thin solid line corresponds to equal selectivity of the exchanger for each of the cations (i.e., a separation factor of unity).

Both the Gapon and modified ideal site-mixing models, which are numerically equivalent, result in normalized binary isotherms that are independent of the presence of a third cat-

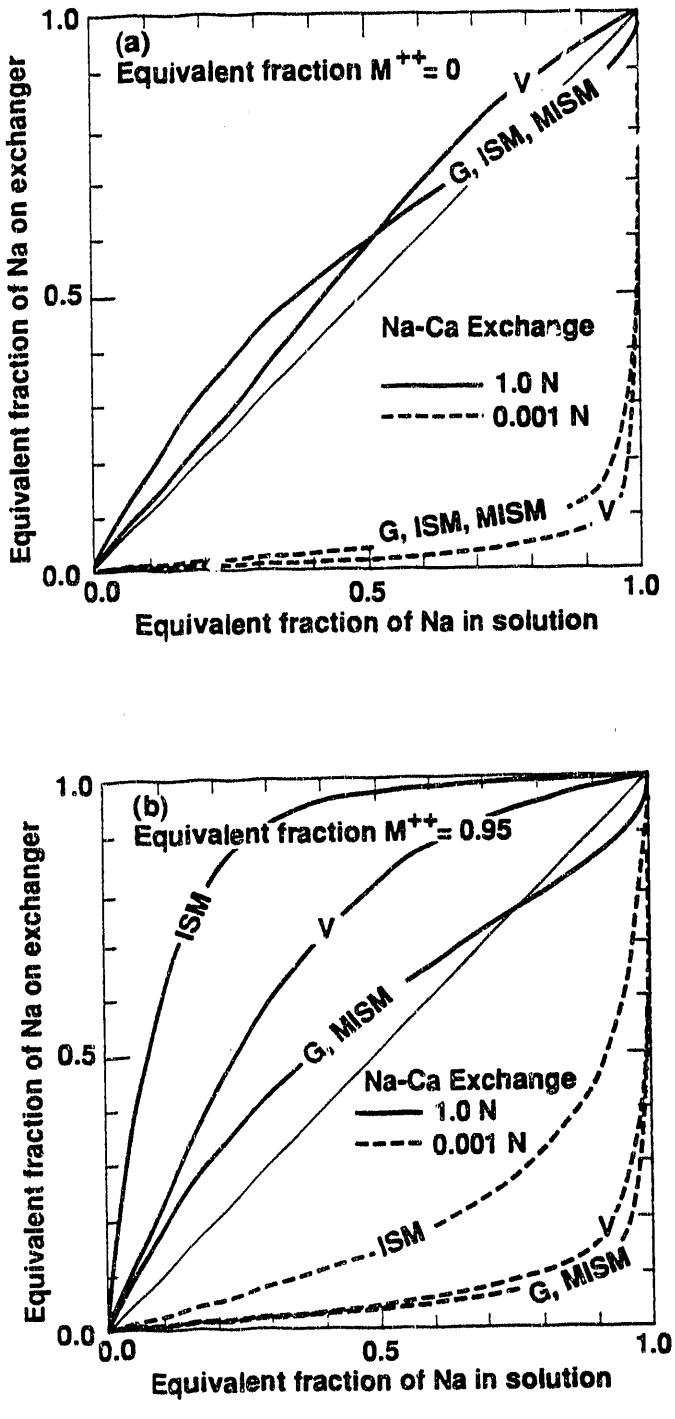

Figure 1. Normalized non-preference Na–Ca binary isotherms for Vanselow (V), Gapon (G), ideal site-mixing (ISM), and modified ideal site-mixing (MISM) models at 1.0 and 0.001 N. (a) Non-binary divalent cation (M^{++}) present at equivalent fraction of 0.0. (b) M^{++} present at equivalent fraction of 0.95. Thin solid line represents separation factor of unity.

ion on the exchanger. In contrast, both the ideal site-mixing solid-solution model and the Vanselow exchange convention predict binary cation-exchange equilibria that are dependent on the concentration of other cations on the exchanger. These models predict that the selectivity of the exchanger for the monovalent cation in a heterovalent exchange will increase as the concentration of other cations (or vacancies) in the exchanger increase. It should be pointed out that if only homovalent exchange was considered, all of the above models would be identical.

Exchangers with multiple exchange sites – Clinoptilolite is known from crystallographic analysis to be composed of more than one type of exchange site. In some cases, exchange isotherms for multisite exchangers that cannot be modeled using a *single–site* ideal model, may be adequately treated by using a *multisite* ideal model (Barrer, 1978). The cation-exchange models in EQ3/6 allow the simulation of ion-exchange when up to three *independent* exchange sites are present in an exchanger if the relative proportion and the cation-exchange energies of each site are known. For multisite minerals, *a single-site non-ideal model* may fit an exchange isotherm equally well as a multisite ideal model (Viani and Bruton, 1992). However, applying a single–site non–ideal model to a multisite exchangers is not warranted unless it is demonstrated that all the exchange sites are energetically equivalent.

Water of hydration and thermodynamic properties of clinoptilolite

For some exchangers, such as zeolites and smectites, the process of exchange of one cation for another may be accompanied by a change in the number of waters of hydration associated with the exchanger and/or cation. As a first approximation to the solid-solution and cation-exchange models, we have assumed that hydration water does not play a role in the thermodynamics of the *exchange reaction*. This assumption is strictly valid only if each clinoptilolite end-member component has the same number of waters of hydration. We chose to assume that the numbers of waters of hydration are the same for each component and are equal to the number of waters measured by Johnson et al. (1991) for clinoptilolite equilibrated at a relative humidity of 50%.

Although the reported exchange energies used to compile the data in Table 3 were derived from binary isotherms without explicitly taking into account exchange of water, the effect of neglecting the transfer of water on the energies of exchange deduced from isotherms is small (Laudelot et al., 1971; Sposito, 1981). For modeling cation–exchange and solid–solution equilibria at 25 °C, explicit accounting for the water of hydration is unnecessary because the exchange energies used to develop the solid–solution component properties were measured at this temperature.

Because the reference reaction (Eq. (C.1)) used to estimate entropy and heat capacity function coefficients explicitly includes the water transferred in going from the natural clinoptilolite to a homoionic end-member, estimates of these quantities are sensitive to the amount and properties of water transferred during exchange. Until the thermodynamic properties of hydration water, the net change in water accompanying exchange, and the temperature dependence of water content are explicitly accounted for in the reference reaction used to derive the heat capacity and entropy of component end-members, solid-

solution properties at elevated temperatures should be considered very tentative. A preliminary assessment of the effect of water of hydration on the solid solution properties at elevated temperatures has been made and will be reported in the future.

Model Validation

The solid–solution and ion–exchange models and data described above were evaluated by comparing predicted stabilities and exchangeable cation distributions of clinoptilolites with: 1) published binary exchange data; 2) compositions of coexisting clinoptilolites and formation waters at Yucca Mountain; 3) experimental sorption isotherms of Cs and Sr on zeolitized tuff; and 4) high temperature experimental data.

Ion-exchange simulations described in the following sections were carried out using version 3245.R116 of EQ3, version 3245.R106 of EQ6, and version 3245.R141 of EQLIB to which the cation exchange options were incorporated. Aqueous species corresponding to the ion–exchanger components were added to version data0.R19 of the thermodynamic data base GEMBOCHS.

Binary exchange in clinoptilolite

Ames (1964a,b) derived the free energy of Na–Ca and Na–K exchange in clinoptilolite from binary isotherms at 25 °C in 1 N chloride solutions. The cation-exchange model based on the Gapon convention was combined with Ames' exchange energies (Table 3) to calculate predicted exchange isotherms for comparison with Ames' experimentally–derived isotherms.

Isotherms predicted assuming a single exchange site (dashed curve) and two exchange sites (solid curve) are shown in Figures 2a and 2b for Na–Ca and Na–K exchange at 25 °C, respectively. A two–site model was developed to better match experimental isotherms and observed K–Ca ratios in clinoptilolites and waters at Yucca Mountain (see below). It was assumed that clinoptilolite consisted of two sites, one with a higher preference for K, the other with a higher preference for Na and Ca, in the relative proportion of 0.4:0.6, respectively. This proportion is consistent with x–ray crystallographic analysis of natural clinoptilolite that indicates that of the three sites occupied by exchange cations, one is predominantly occupied by K and the other two are predominantly occupied by Na and Ca (e.g., Smyth et al., 1990). The energies of Na–Ca and Na–K exchange on each site were adjusted, subject to the constraint that the overall energy of exchange equaled Ames' values, until the predicted isotherms visually matched the data (Table 4).

The shape of the isotherms defined by the experimental data points is well reproduced by the predicted curves, which tends to support the validity of the exchange models. It appears that this modeling approach with either the one- or two-site cation-exchange models can reasonably describe available experimental data for clinoptilolite.

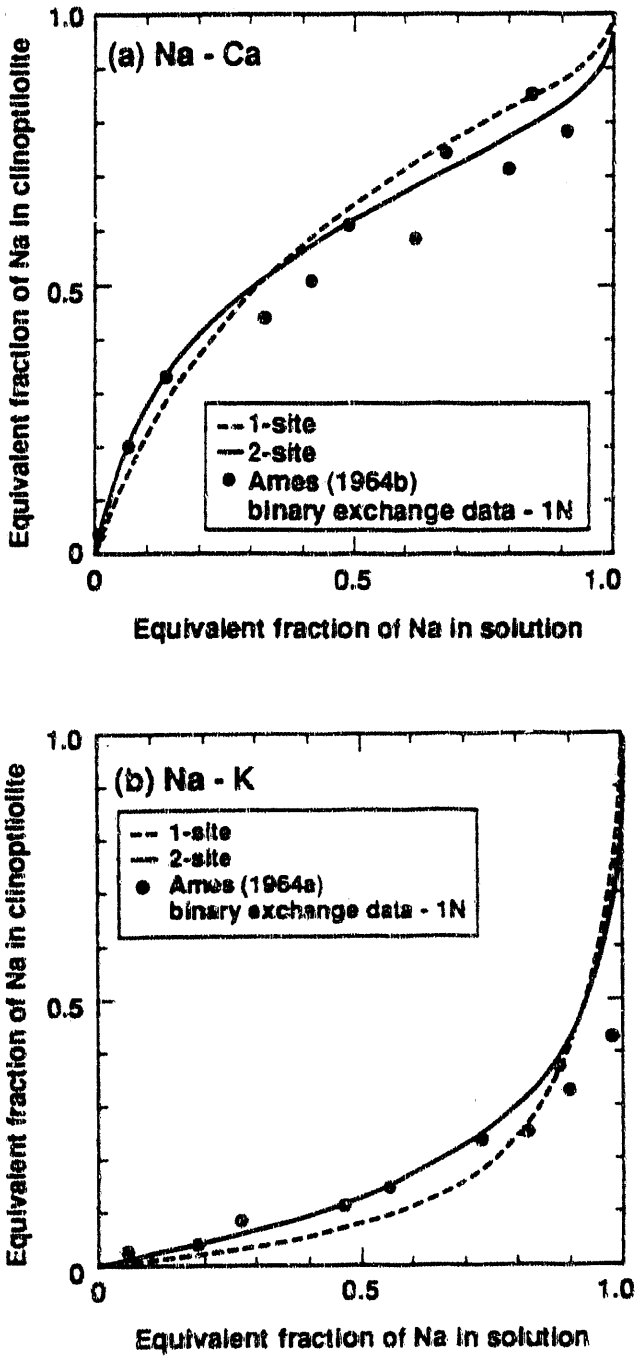

Figure 2. Binary exchange data from Ames (1964a,b) in 1 N solution at 25 °C (filled circles) compared to exchange isotherms predicted using the one–and two–site Gapon convention models (dashed and solid curves; see text). (a) Na–Ca, (b) Na–K.

Table 4. Parameters used in two-site exchange model

Site	Fraction[1]	Exchange energy, kcal/equiv	
		Na —> K[2]	Na —> ½ Ca
Site 1	0.4	-0.6	-0.75
Site 2	0.6	-2.1	0.583
Total	1.0	-1.5[3]	0.05[3]

(1) Fraction of total *equivalents* on each site.
(2) Na —> K symbolizes the exchange reaction: Na-clinoptilolite + K^+ = K-clinoptilolite + Na^+.
(3) Exchange energy for complete exchange over both sites (from Table 3).

Correlations between clinoptilolite composition and formation water chemistry at Yucca Mountain

Chemical analyses of waters sampled from wells penetrating the saturated zone at Yucca Mountain, Nevada can be used to predict the exchangeable cation distribution of clinoptilolites in equilibrium with the waters. The predicted compositions can then be compared to the compositions of clinoptilolites sampled from the same wells at equivalent depths. Binary exchange isotherms can also be calculated for comparison with compositional data for clinoptilolites sampled from Yucca Mountain wells.

Calculated normalized binary exchange isotherms for Na-Ca and K-Ca exchange in clinoptilolite at 25°C are shown in Figures 3a and 3b, respectively. Exchange was modeled in J-13 water (Delany, 1985) using the Gapon convention. J-13 water was chosen to be representative of saturated zone waters across Yucca Mountain. Predictions for both one-site and two-site models are shown.

The vertical bars in Figure 3 represent the range in observed exchangeable cation distributions of clinoptilolites in a given well at depths corresponding to those from which the fluid samples were obtained. Multiple fluid samples from a given well were sufficiently similar that their equivalent fraction of cations in solution were essentially equal. Equivalent fraction was referenced to the sum of the equivalents of Na+Ca or K+Ca in each phase. Chemical analyses of waters sampled from wells J-13, UE25 b-1, UE25 P-1, USW G-4, USW H-4 and USW H-5 which penetrate the saturated zone were obtained from Benson et al. (1983), Ogard and Kerrisk (1984) and Benson and McKinley (1985). Chemical compositions of clinoptilolites from the same wells were selected from Levy (1984) and Broxton et al. (1986) to best represent the depth intervals from which the water samples were obtained.

The one- and two-site models fit the data for Na-Ca exchange fairly well (Figure 3a). Although the one-site model does not reproduce observed data for K-Ca exchange (Figure 3b), the two-site model, which incorporates a site with a high affinity for K (Table 4),

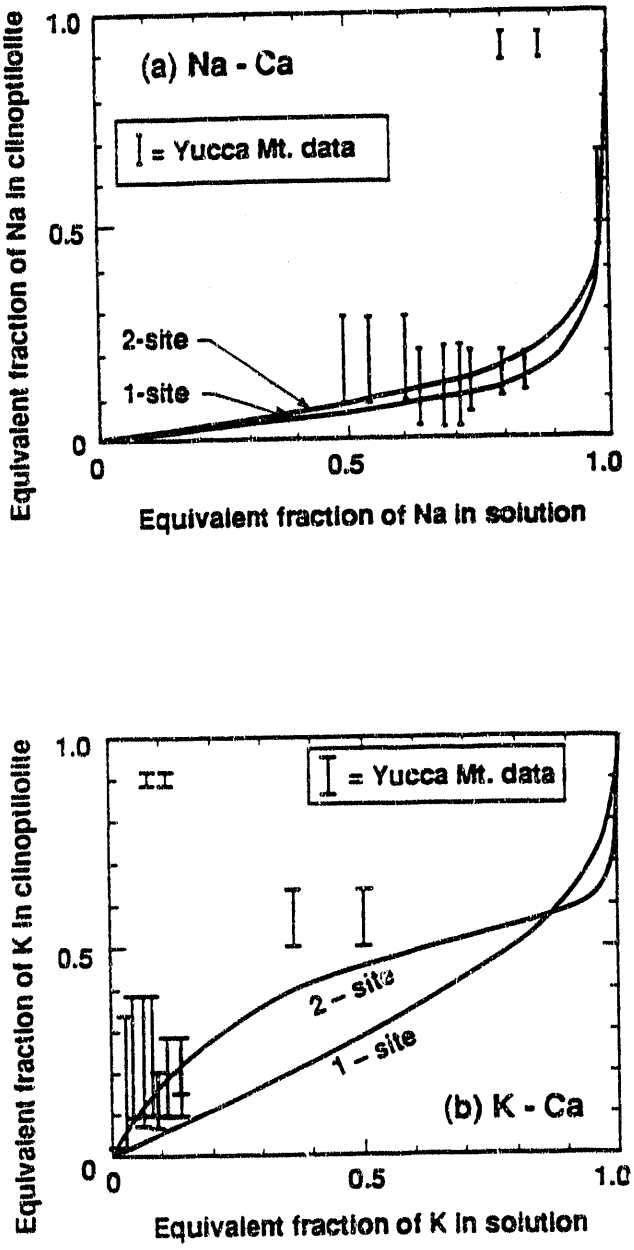

Figure 3. Predicted exchange isotherms at 25 °C. (a) Na–Ca exchange at a total normality of Na plus Ca in J–13 water of 0.00253. (b) K–Ca exchange at a total normality of K plus Ca in J–13 water of 0.000755. Isotherms are shown for both one– and two–site models using the Gapon convention. Vertical bars represent correlations between analyzed compositions of formation waters and clinoptilolites at Yucca Mountain (see text). The vertical bars at highest equivalent fractions of Na or K in clinoptilolite represent data for well USW H–4.

better matches observed compositions of clinoptilolite and water. This is consistent with experimental data showing that K is not exchanged freely once it has entered the exchange site (Bish, 1984, 1988).

Data for well USW H–4, located at the highest equivalent fractions of Na and K in Figure 3, fall far off both exchange isotherms. Clinoptilolites from the Prow Pass member of the Crater Flat Tuff of well USW H–4 have relatively low Ca contents. However, the fluid chemistry does not seem to reflect the observed compositional differences. The apparent disequilibrium between the low-Ca clinoptilolites and nearby waters should be examined further; in particular, the possibility that the two are not in direct contact should be evaluated.

The match between predicted and observed clinoptilolite compositions with water chemistry from a selected series of Yucca Mountain wells is depicted in Figure 4. The combinations of clinoptilolites and fluid analyses were selected as the best available matches between the depths represented by the fluid sample and the depth from which the clinoptilolite was obtained. The one-site Gapon cation-exchange model, equivalent to the modified ideal site-mixing model, was used to calculate the mole percent of Na on the exchange site in clinoptilolite assuming equilibrium between clinoptilolite and the adjacent pore fluid.

A wide range of clinoptilolite compositions was measured from each depth zone of interest, as reflected in the horizontal extent of the symbols in Figure 4. In contrast, the fluid compositions from each well were similar, as reflected in the small range in predicted clinoptilolite compositions. A perfect correspondence between the observed and predicted compositions would fall on the solid line with a slope of one.

The cation-exchange and solid-solution models are generally consistent with observed compositional data. However, data from well USW H–4 show large deviations from predicted compositions because of the low Ca content of waters from this well. The range in natural data suggest that it is important to account for different generations and occurrences of clinoptilolite. Although clinoptilolite would be expected to exchange rapidly with surrounding pore waters, Figure 4 as well as Figure 3 show that wide variations in clinoptilolite composition seem to exist in the absence of correspondingly large variations in fluid composition.

It is possible that chemistries of sampled waters do not accurately reflect small-scale variations in in-situ fluid chemistries. In addition, we cannot be sure that the sampled fluids were actually in contact with the clinoptilolites for which compositional data is available. There is poor correspondence between wells with fluid chemistry data and those with data on clinoptilolite exchange cation distributions. Future work should seek to relate the variability in the exchangeable cation distribution of clinoptilolite to the mineralogic, petrologic and transport characteristics of the host rock as well as to the compositions of sampled fluids.

The preference of clinoptilolite exchange site(s) for K relative to one-site model predictions is illustrated in Figure 5. Figure 5 summarizes the exchangeable cation distribution of clinoptilolites from the saturated zone at various Yucca Mountain drill sites (filled

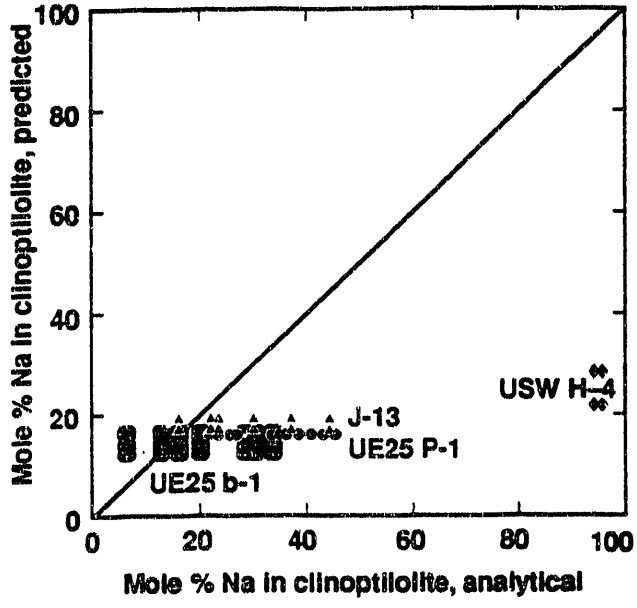

Figure 4. Comparison between predicted and analytical compositions of clinoptilolites at Yucca Mountain for wells UE25 b-1, UE25 P-1, J-13 and USW H-4 (see text).

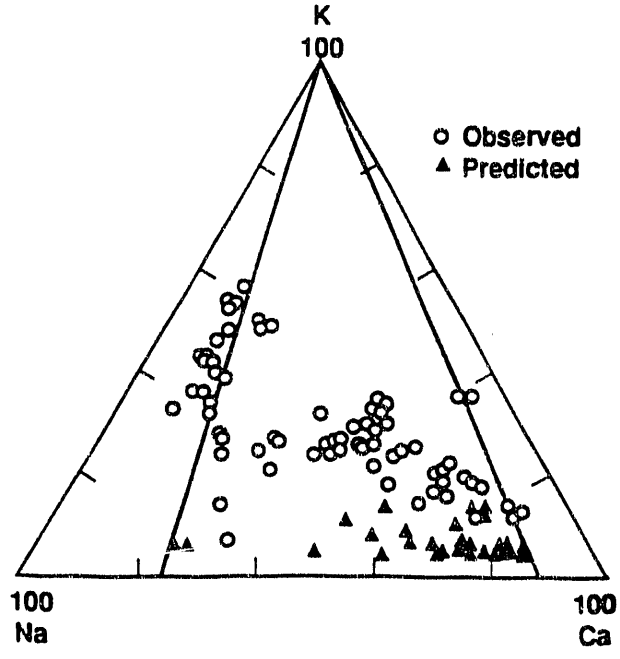

Figure 5. Ternary plot comparing analyzed exchangeable cation distributions of clinoptilolites from the saturated zone at Yucca Mountain (open circles) with predicted clinoptilolite compositions (filled triangles). The one-site Gapon model was used. Clinoptilolite compositional data from Levy (personal commun., 1990); clinoptilolite compositions predicted from water compositional data from Benson et al. (1983), Ogard and Kerrisk (1984) and Benson and McKinley (1985).

circles; Levy, personal commun., 1990). The compositions of fluids from the saturated zone across Yucca Mountain were used to predict the exchangeable cation distributions in coexisting clinoptilolites for comparison (filled triangles). The one-site Gapon convention model was used.

Predicted compositions of clinoptilolite approximately span the range of observed Na–Ca ratios, as shown by the bounding lines leading to the K apex in Figure 5. However, natural clinoptilolites are significantly enriched in K relative to predicted compositions. Further refinement of the models is required to provide adequately for the preference of clinoptilolites exchange site(s) for K. A future report will detail results obtained using a two–site model.

Partition coefficients and sorption isotherms for Cs and Sr on Yucca Mountain tuff samples

Experimental measurements of the extent of sorption of Cs and Sr on tuff from Yucca Mountain were compared with sorption predicted using the cation-exchange option in EQ3. The experimental sorption data base consisted of partition coefficients and sorption isotherms obtained from batch experiments using samples of crushed tuff and groundwater from well J-13.

Predicted vs. measured partition coefficients – The partition coefficient, K_d, is defined as

$$K_d = \frac{c_{ads}}{c_{sol}} \quad , \tag{14}$$

where c_{ads} and c_{sol} represent the concentration of the element adsorbed to the solid phase and in the solution at equilibrium, respectively. When c_{ads} and c_{sol} are expressed in units of micromol/g and micromol/mL, K_d has units of mL/g. K_d's can be readily computed from the equilibrium cation-exchanger and solution compositions output from EQ3 modeling runs.

A series of EQ3 runs were made to predict K_d's for Yucca Mountain tuffs for which measured Cs and Sr K_d's (Fuentes et al., 1987), cation-exchange capacity (CEC), composition of the exchangeable cations (Thomas, 1987), and X–ray diffraction (XRD) estimates of mineral abundances (Chipera and Bish, 1989) were available. The reported CEC and XRD data and experimental solid:solution ratio were used to compute the equivalents of exchanger/kg H_2O input for each modeling run. The initial composition of the exchanger was set equal to the measured exchange cation distribution. Exchange was modeled using the Vanselow convention and assuming a single exchange site.

For some samples a significant fraction of the exchange capacity was due to smectite. To model sorption in these samples smectite, with exchange energies reported for a Wyoming-type montmorillonite (Gast, 1972; Fletcher and Sposito, 1989), was included in the EQ3 runs. The portion of the measured exchange capacity of the sample due to each exchanger was calculated from their relative abundance and the CEC of the pure exchanger

phases by assuming that only the identified exchanger phases contributed to the measured exchange capacity. CEC values for clinoptilolite and smectite, appropriate to Yucca Mountain tuffs, were obtained by a multilinear regression of the measured exchange capacities and mineral abundances reported by Thomas (1987) and Chipera and Bish (1989). The CEC estimates obtained, 2.12 and 0.85 mequiv/g for clinoptilolite and smectite, respectively, are consistent with commonly reported values for these minerals. Table 5 summarizes the experimental data and model inputs for a sample run.

Figures 6a and 6b compare K_d's computed from EQ3 modeling runs with the experimentally measured values for Cs and Sr. Each point represents a single EQ3-run / experimental-measurement pair. Filled and open circles represent samples in which > 90% of the exchange capacity was attributable to clinoptilolite and smectite, respectively. The dashed line represents 1:1 correspondence between measured and predicted K_d's. There is good agreement between model prediction and measurement for Sr sorption over a wide range in K_d values. For Cs, the model underestimates K_d's for most of the smectite-rich samples and for samples with low CEC's.

The distinct non-ideality of Na–Cs exchange on smectites noted by Gast (1972) suggests that multiple exchange sites exist in smectites, some of which have a much greater affinity for Cs. The underestimation of Cs K_d's for the smectite-rich samples may arise because the exchange energies used in the modeling represent the overall energies of exchange and do not reflect the high affinity that some sites have for Cs. An alternative, or contributing reason for the underestimation of Cs K_d's may be due to neglecting the sorptive capacity of the small amounts of mica (illite?) identified (but not quantified) in these samples. Brouwer et al. (1983) have shown that Cs exchange on illite is best modeled as occurring on three sites, one of which has a very high affinity for Cs. Given information about the abundance of high-affinity exchange sites for Cs on smectite and/or illite, improved correspondence between modeling results and experimental measurements would be expected.

Predicted vs. measured sorption isotherms for Cs and Sr on a clinoptilolite-bearing sample of the Bedded Tuff of Calico Hills – In Figures 7a and 7b, measured sorption isotherms for Cs and Sr on sample YM–38, shown as filled circles, are compared with the isotherms predicted using EQ3, shown as solid lines. The predicted isotherms were computed using a single-site Vanselow model, the measured sample CEC and exchangeable cation composition (Thomas, 1987), and the reported *total* concentrations of Cs and Sr (Fuentes et al., 1987). The agreement between model and measurement is excellent and suggests that adsorption of trace quantities of Cs and Sr at 25 °C can be adequately modeled using a simple single–site model and available cation-exchange data.

Table 5. Parameters used to model sorption of Cs and Sr on Yucca Mt. tuffs using EQ3/6: Example using sample YM-38.

Parameters required for modeling	Value of parameter used in, or measured by, experiment (1)	Value used for EQ3 input or to calculate input parameters
Solid : solution ratio	1 g : 20 mL	50 g : kg H_2O
Fluid composition		
Composition of background solution	J-13 Well Water	J-13 Well Water (2)
Initial concentration of Cs and Sr tracers	As reported	As reported
Exchanger abundance		
Clinoptilolite	64 wt-%	As reported
Smectite	5 wt-%	"
Exchange capacities		
Whole sample	1.22×10^{-3} equiv/g	0.061 equiv/kg of H_2O (3)
Due to clinoptilolite	Not measured	0.0591 equiv/kg of H_2O (4)
Due to smectite	"	0.0019 equiv/kg of H_2O (4)
Initial composition of exchanger(s)	Na 21.0 equivalent-% K 32.9 " Ca 46.1 "	As reported
Exchange energies		
Clinoptilolite exchanger	Not used	Na —> Cs -2.33 kcal/equiv (5) Na —> Sr -0.05 " Na —> Ca 0.05 " Na —> K -1.50 "
Smectite exchanger	Not used	Na —> Cs -1.081 kcal/equiv Na —> Sr -0.116 " Na —> Ca -0.116 " Na —> Mg -0.116 " Na —> K -0.348 "
Exchanger model	Not used	Vanselow, one-site

(1) Experimental data from Chipera and Bish (1989), Fuentes et al. (1987), and Thomas (1987).

(2) Composition of J-13 from Delany (1985).

(3) This value computed as follows: $0.061\ equiv/kg\ of\ H_2O = (1.22 \times 10^{-3}\ equiv/g) \times (50.0\ g/kg\ of\ H_2O)$

(4) Exchange capacities due to the individual exchangers were calculated using mineral abundances and the exchange capacities of the pure exchangers, and by assuming the sample CEC was due to clinoptilolite and smectite only. For example, the exchange capacity due to the smectite component is calculated according to:

$$0.0019\ equiv/kg\ of\ H_2O = \frac{(5\% \times 0.85\ mequiv/g)}{(64\% \times 2.12\ mequiv/g) + (5\% \times 0.85\ mequiv/g)} \times (0.061\ equiv/g\ of\ H_2O)$$

where 0.85 and 2.12 are the CEC's for the pure smectite and clinoptilolite, respectively. The latter values were obtained by a multilinear regression of the sample CEC's and mineral abundances.

(5) Exchange energies for clinoptilolite from Table 2; data for smectite from Gast (1972) and Fletcher and and Sposito (1989). Na —> Cs symbolizes the conversion of one equivalent of Na-exchanger to one equivalent of Cs-exchanger.

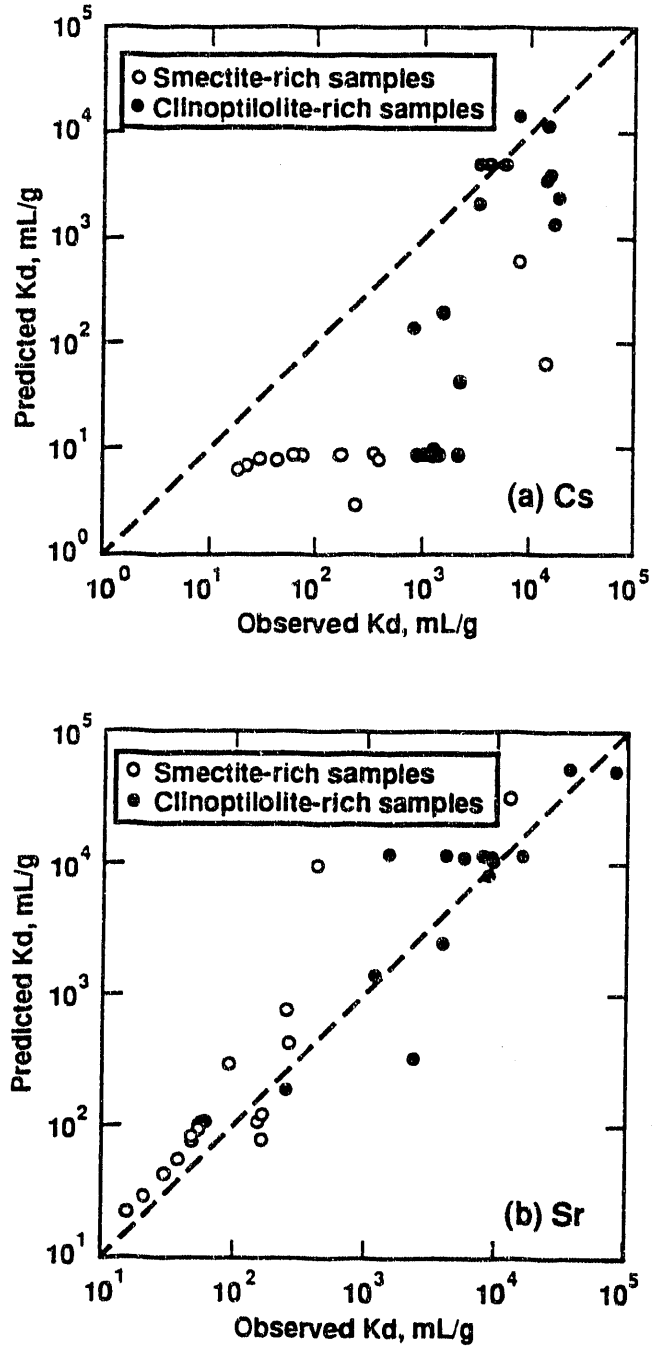

Figure 6. Predicted vs. experimental partition coefficients (K_d) for (a) Cs and (b) Sr on samples of Yucca Mountain tuff. Filled and open circles represent samples in which the exchange capacity is mainly due to clinoptilolite and smectite, respectively. Experimental data from Fuentes et al. (1987). Predictions were made using a one--site Vanselow exchange model. See Table 5 for additional parameters used in the modeling.

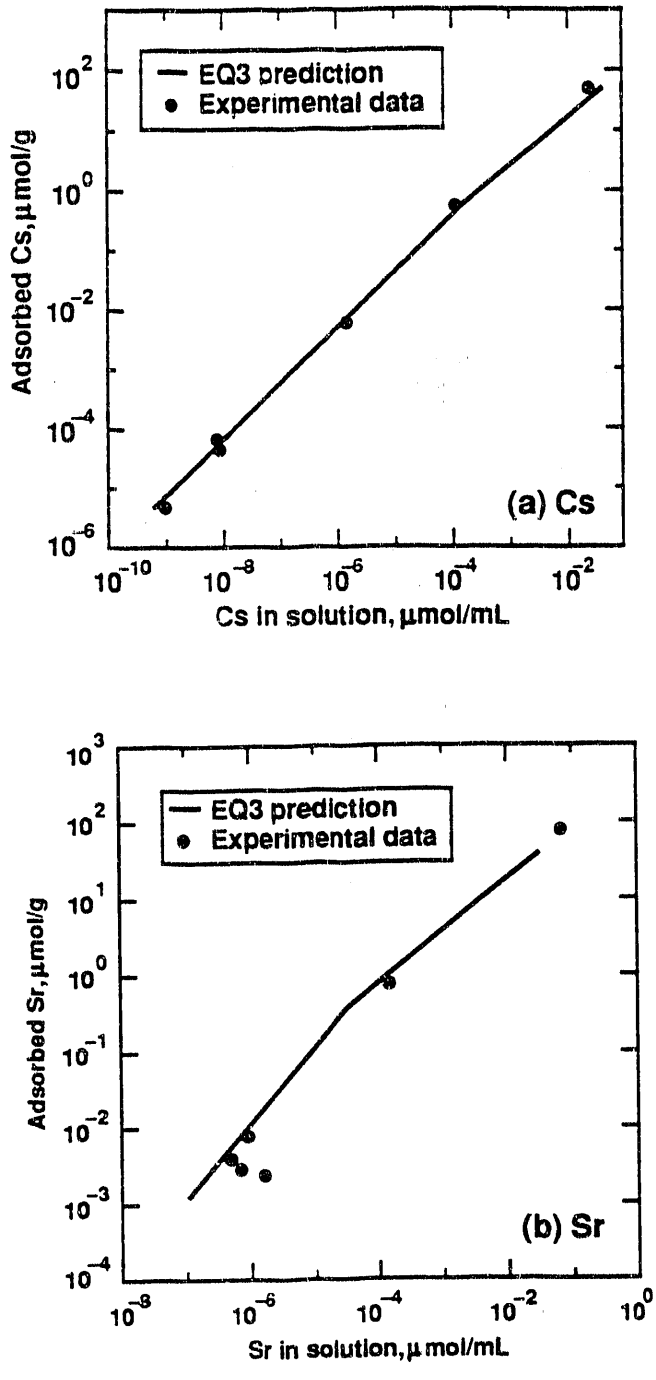

Figure 7. Predicted (solid lines) and experimental (filled circles) isotherms for (a) Cs and (b) Sr on sample YM–38 from the Bedded Tuff of Calico Hills, Yucca Mountain. Experimental data from Fuentes et al. (1987). Predicted isotherms were computed assuming a one–site Vanselow exchange model. See Table 5 for additional parameters used in the modeling.

Effect of composition and abundance of clinoptilolite on predicted K_d's – To examine the relationship between sorption and the distribution of the exchange cations on clinoptilolite, EQ3 was used to predict K_d's for varying abundances of end-member clinoptilolites (Figure 8). K_d's for Cs on clinoptilolite with 100% Na on the cation exchange site are 20 times higher than on clinoptilolite with 100% Ca on the exchange site. It is clear that sorption is very sensitive to clinoptilolite composition and that any attempt to obtain a statistical correlation between clinoptilolite abundance and measured K_d will be confounded by the compositional dependence. This finding also means that changes in clinoptilolite composition that might arise due to interactions with potential repository components must be considered when predicting sorptive capacity. For example, if fluids interact with Ca-rich cement, migrate into surrounding host rock and cause host rock clinoptilolites to become more Ca-rich, the sorptive capacity for radionuclides would decrease.

It is apparent that the equilibrium model we have applied can serve to integrate the mineralogical, solution, and sorption data to a degree impossible using empirical isotherms and/or statistical approaches. The generally good agreement between model predictions and sorption measurements means that the significant mineralogical data base collected by Los Alamos National Laboratory (Bish and Chipera, 1989, Broxton et al., 1986) can be utilized to predict Cs and Sr K_d's for tuffs for which sorption data is lacking. This was not feasible heretofore. Application of the exchange model will also allow predictions to be made concerning the effects of temperature and solution composition on sorption, which are required to model the long-term sorptive behavior of clinoptilolite.

Clinoptilolites in high temperature experiments

Few reliable data exist to test predictions of clinoptilolite exchange site distributions at elevated temperature. One possible test involves an experiment by Knauss and Peifer (1986) in which clinoptilolite was formed when J-13 water was reacted with vitric Topopah Spring tuff at 250 °C. Clinoptilolite precipitates had an exchangeable cation distribution of 32 mole% Ca, 25% Na and 42% K, although the water from which the clinoptilolites precipitated contained no detectable Ca.

Calculations of the relation between the Ca content of clinoptilolite and the Ca concentration in solution using a one-site Gapon model (Figure 9), suggest that concentrations of Ca in solution in equilibrium with clinoptilolite are well below the parts per billion level. Despite the need to provide for a preference for K in the models, the calculations suggest that the models are in accord with high-temperature, experimentally observed water and clinoptilolite compositions.

The effect of temperature on Cs adsorption on clinoptilolite was modeled by calculating the K_d for sample YM–38 of the Calico Hills formation using a single-site Vanselow exchange model (Figure 10). The results predict a significant decrease in Cs sorption with increasing temperature.

Calculations of the stability and exchangeable cation distribution of clinoptilolite at elevated temperatures must be considered provisional, pending the experimental determina-

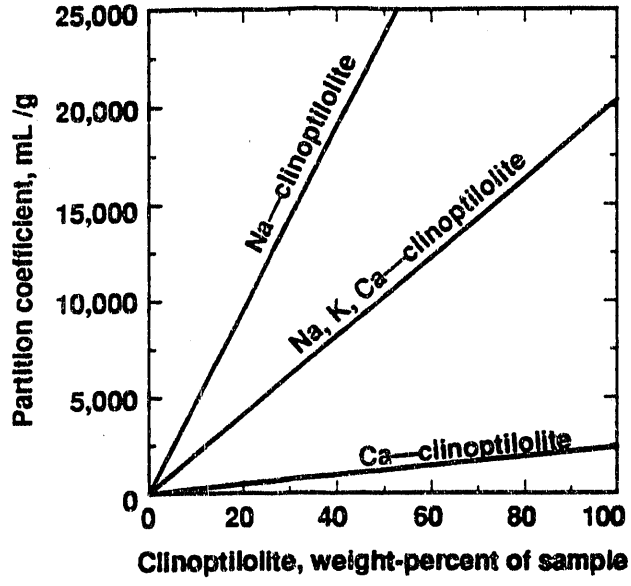

Figure 8. Effect of clinoptilolite composition and abundance on predicted values of the partition coefficient (K_d) of Cs in a clinoptilolite-bearing sample. Na- and Ca-clinoptilolite refer to clinoptilolite with 100% Na and Ca on the exchange site, respectively. Na,K,Ca-clinoptilolite refers to a clinoptilolite whose cation distribution on the exchange site is given in Table 5.

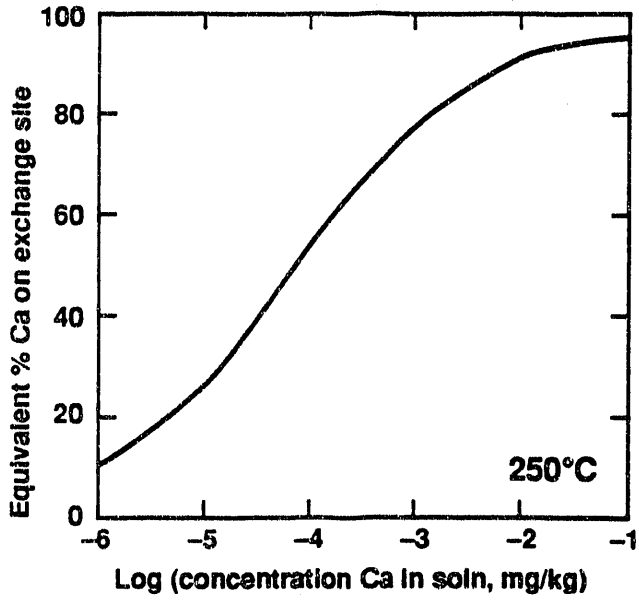

Figure 9. Relation between equivalent percent of Ca on the exchange site of clinoptilolite and the concentration of Ca in solution at 250°C (see text). The one-site Gapon model was used.

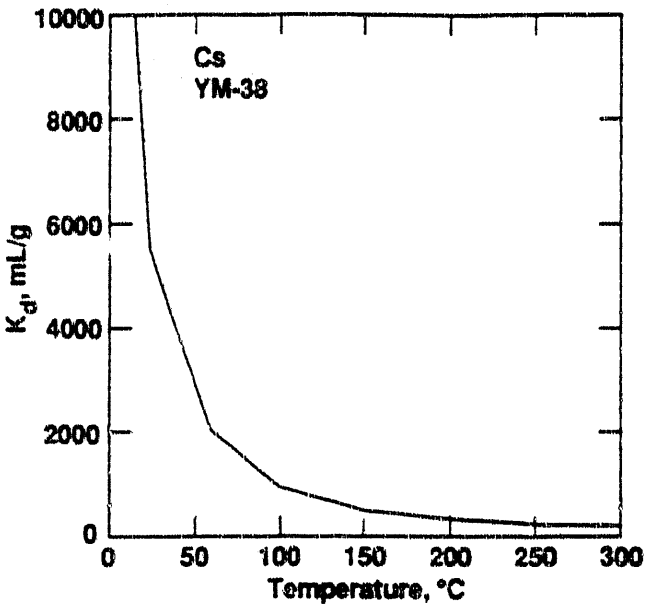

Figure 10. Relation between temperature and Cs K_d predicted using the one-site Vanselow model for sample YM-38 from the Bedded Tuff of Calico Hills in contact with J-13 groundwater.

tion of cation exchange at elevated temperature. As discussed previously, the heat capacity power functions of the homoionic end-members in the clinoptilolite solid-solution model were estimated in the absence of such data by utilizing a "summation of oxides" approach and by assuming the water of hydration was equal and invariant with temperature for each end-member.

Effects of Temperature and Ionic Strength on Exchangeable Cation Distribution

The solid-solution and ion-exchange models for clinoptilolite can be used to provide a first approximation of how the exchangeable cation distribution of Yucca Mountain clinoptilolites may change when the rock heats in response to waste package emplacement. Formation waters may not only increase in temperature, but also increase in salinity if evaporation or boiling occurs. Using the estimates of the heat capacity of the clinoptilolite end-members, the exchange isotherms for Na–Ca exchange in 0.001 N solutions (similar to Yucca Mountain) and 1.0 N solutions at 25° and 100°C were calculated using the one-site Gapon model (Figure 11a).

At 25°C and 0.001 N, Ca is favored over Na in the exchange site at all solution compositions (Figure 11a). At 100°C, the preference for Ca is even more pronounced. Increasing temperatures at Yucca Mountain would, therefore, favor the stability of Ca-rich clinoptilolites relative to Na-rich clinoptilolites. Accordingly, Ca will tend to replace Na on the exchange site as temperatures increase.

The effects of increasing ionic strength at 25°C from 0.001 N to 1.0 N are shown in both Figures 11a and 11b. Increasing ionic strength favors Na and K rather than Ca in the exchange site. The preference of clinoptilolite for Na and K at increased ionic strength would thus be opposed to its preference for Ca at increased temperature.

Future Work

Further work is required in order to make dependable predictions of the sorptive behavior of clinoptilolite under varying physical and chemical conditions. For example, changes in the composition of clinoptilolite due to cation-exchange may be accompanied by changes in the waters of hydration. The energetic effects of this phenomenon is not known, yet must be provided for in order to predict both sorption behavior and phase stability. The cation-exchange and solid-solution models for clinoptilolite must also be refined in order to provide for a preference for K on the exchange site(s) of clinoptilolite. Critical need exists for experimental data on energies of ion exchange, especially for radionuclides of interest, at 25°C and elevated temperature. Despite our success in modeling Cs and Sr exchange on clinoptilolite, our predictions are limited to 25°C until exchange data at higher temperatures can be obtained.

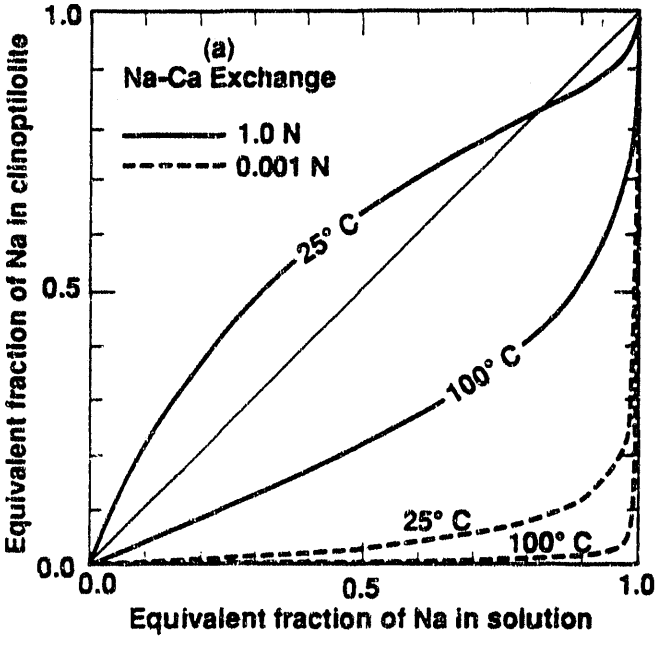

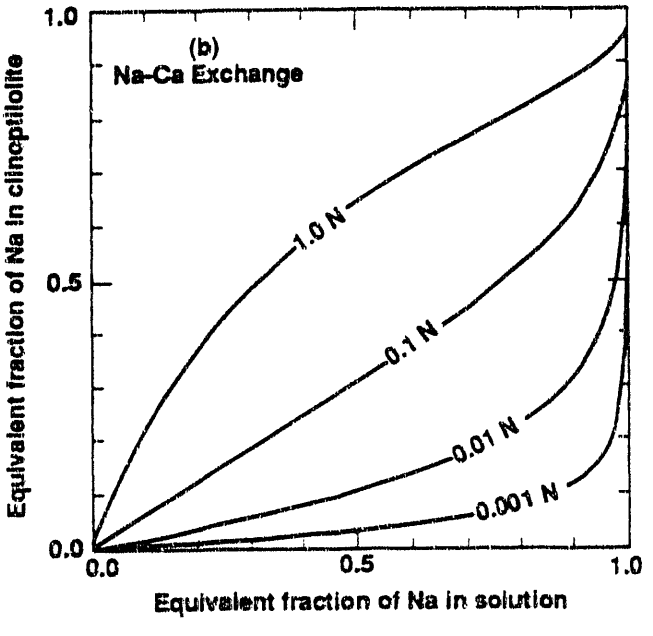

Figure 11. Predicted adsorption isotherms for Na–Ca exchange on clinoptilolite assuming a one-site Gapon model. (a) 0.001 and 1.0 N solutions at 25 and 100 °C. (b) 0.001 to 1.0 N solutions at 25 °C.

II. Geochemical Simulation of Fluid-Rock Interactions at Yucca Mountain

Introduction

Numerical simulations describing how mineral assemblages and fluid compositions may change over the lifetime of the potential Yucca Mountain repository need to be conducted to address conditions that are not represented by laboratory experiments. Results of preliminary efforts at simulating the chemical evolution of repository host rock minerals and fluids are presented in this section to place bounds on the range of possible reaction products that may develop for expected ranges of water compositions.

Geochemical simulations described in the following sections were carried out using version 3245.R124 of EQ3, version 3245.R119 of EQ6 and version data0.com.R7 of the thermodynamic data base GEMBOCHS.

Controls of Mineral Evolution at Yucca Mountain

The stability of host rock minerals and the potential for mineralogical reactions will be influenced by changes in temperature that occur when waste packages are emplaced in the potential repository. The thermal response of clinoptilolite is of particular interest because of its potential impact on the permeability of clinoptilolite-rich zones, and on the cation exchange capacity and composition of clinoptilolite.

Diagenetic reactions in natural systems can be used as a natural analogue for "man-made" diagenetic reactions that may occur around an emplaced waste package. In particular, the sequence of diagenetic mineral assemblages with depth in silicic tuffs at Yucca Mountain can be used as a natural analogue for the response of tuff to increased temperature. Broxton, Bish and Warren (1987) identified the following diagenetic zones with depth at Yucca Mountain.

- Zone 1 - glass, opal, smectite, cristobalite, clinoptilolite
- Zone 2 - opal, cristobalite, quartz, clinoptilolite, mordenite, authigenic K-feldspar and smectite
- Zone 3 - quartz, analcime, authigenic K-feldspar, smectite, smectite/illite, calcite
- Zone 4 - quartz, authigenic K-feldspar and albite, smectite, calcite, plus minor chlorite, epidote and iron oxides

Kerrisk (1983) and Duffy (1984) postulated that the activity of aqueous silica (SiO_2(aq)) controls the observed mineralogical zones at Yucca Mountain. They suggest that the activity of SiO_2(aq) is controlled by the identity of the solid SiO_2 polymorph and the kinetics of transformation of the SiO_2 polymorphs from glass to quartz. The generalized sequence of silica polymorphs with increasing depth at Yucca Mountain is: glass → opal -CT/cristobalite → quartz. They postulate that clinoptilolite occurs when SiO_2(aq) is buffered at high values by glass or cristobalite, and analcime and albite develop when it is buffered at lower values by quartz. The sequence clinoptilolite → analcime → albite observed at Yucca Mountain is a common burial diagenetic sequence in volcanic rocks (Iijima, 1988).

Diagenetic reactions in the Yucca Mountain volcanic rocks with depth were simulated using EQ3/6 to evaluate the relationship between the identity of the silica polymorph and the diagenetic assemblage. In this study, the overall stability of the clinoptilolite solid solution was evaluated at the same time as the exchange cation occupancies were computed as a function of both temperature and the identity of co-precipitates.

The diagenetic evolution at Yucca Mountain was simulated by reacting glass shards with rain water in a closed system from 25 to 90°C. The glass composition was assumed to be that of a brown glass shard from the Topopah Spring Member of the Paintbrush Tuff from well H-5 (Levy, 1984). The glass shards were assumed to dissolve congruently in the dilute rainwater. Glass dissolution proceeded linearly with temperature, such that 1 mole of glass was dissolved in 1 kilogram of water as the temperature increased from 25 to 90°C. The extent of reaction was tracked by the amount of glass dissolved and the temperature, rather than explicitly in terms of time.

The identity of the silica polymorph was controlled at each step in the simulation. Glass was allowed to dissolve as temperature increased with burial until saturation with amorphous silica was achieved. Aqueous silica concentrations in metastable equilibrium with amorphous silica approximate those in contact with glass. Shortly thereafter, cristobalite precipitation was allowed to begin in order to decrease the SiO_2(aq) activity in solution. When the temperature reached 90°C, which is below the 96°C boiling point at Yucca Mountain, quartz was allowed to precipitate in order to further decrease the SiO_2(aq) activity. At 90°C, glass dissolution continued congruently, although temperature was held constant.

The diagenetic sequence of events predicted to occur during burial of glass shards in contact with rain water is shown in Figure 12a. Despite the fact that the kinetics of transformation of the SiO_2 polymorphs were not included explicitly in the simulations, the predicted diagenetic sequence agrees favorably with the observed diagenetic zones I, II, III and IV at Yucca Mountain (Broxton, Bish and Warren, 1987). Diagenetic zones I, II and IV are well represented by the amorphous silica, cristobalite and quartz zones, respectively. Diagenetic zone III is not represented in the simulation because of the absence of analcime, whose thermodynamic data may not provide adequately for its compositional variability. The correspondence between observed and predicted mineralogical assemblages supports the contention that the identity of the silica polymorph and the corresponding activity of SiO_2(aq) control diagenetic evolution at Yucca Mountain.

The composition of clinoptilolite changed continuously during the interval of clinoptilolite precipitation shown in Figure 12a. The evolution of the exchangeable cation distribution in clinoptilolite that precipitated during the simulation is shown in Figure 12b. Predicted clinoptilolite compositions are generally Na-rich and Ca-poor. The proportion of Ca was low because the zeolite stilbite precipitated and sequestered much of the available Ca. As discussed in Appendix E, the thermodynamic data for stilbite suggest that stilbite is stable in fluids with a wide range of chemical compositions. Future work should be directed to ascertaining the stability of stilbite relative to other zeolites from natural occurrences and abundances.

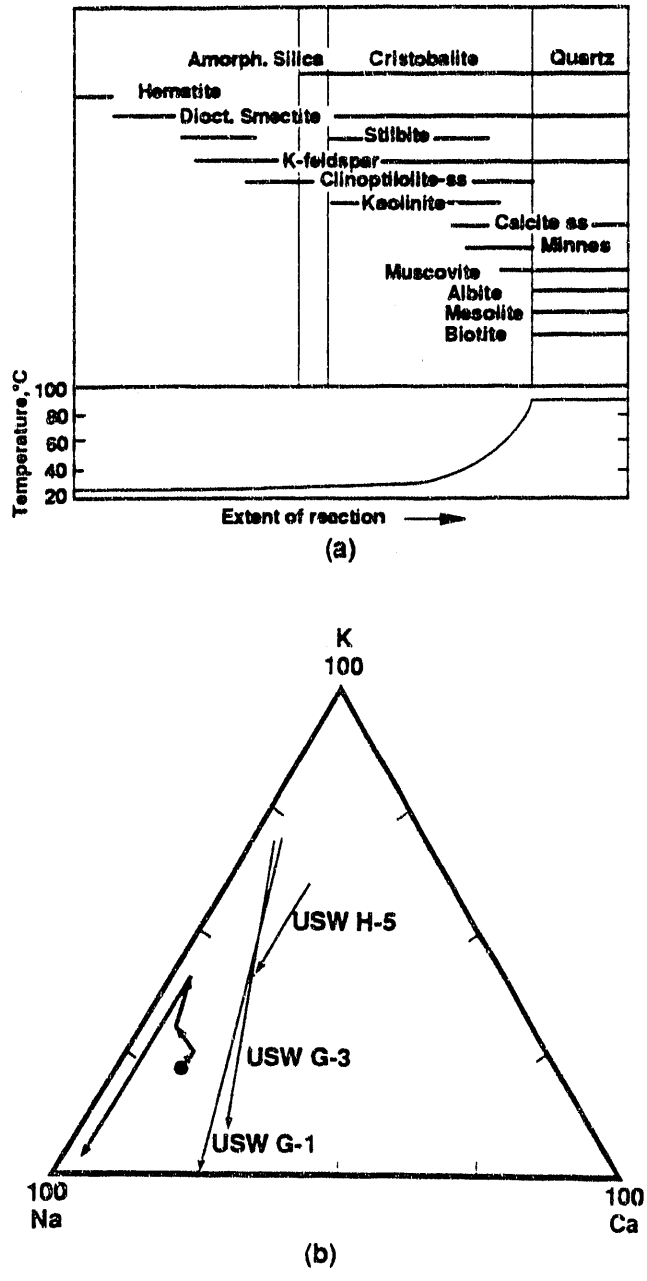

Figure 12. Simulation results for reaction of Topopah Spring glass shards with J-13 water from 25 to 90°C. (a) Predicted paragenetic sequence. Horizontal "lines" delineate regions of stability for solid phases as labelled. The uppermost "line" represents the stepwise conversion of the silica polymorph from amorphous silica to cristobalite to quartz (see text). Dioct. = dioctahedral, ss = solid solution, Minnes = minnesotaite (Fe-rich aluminosilicate). Biotite and minnesotaite can be considered as proxies for the Fe-rich chlorite, epidote and iron oxides in diagenetic zone IV. (b) Ternary diagram comparing predicted variation in Na-K-Ca exchangeable cation distribution in clinoptilolite, in mole percent, with observed compositional trends with depth in Yucca Mountain wells USW H-5, USW G-1 and USW G-3 (light lines). Filled circle represents start of simulation; arrowheads show evolution of clinoptilolite composition.

Predicted compositional trends of clinoptilolite agree well with observed trends with depth of exchangeable cations in clinoptilolite-group minerals from diagenetic zones II and III at Yucca Mountain. The wells represented in Figure 12b are classified as the western alkalic group, whose waters are not believed to be mixed with waters from underlying Paleozoic carbonate aquifers (Broxton, Bish and Warren, 1987).

Predicted clinoptilolite precipitates contain as much as 41 mole-% K (Figure 12b), even though it was shown previously that our cation-exchange and solid-solution models need to be refined in order to describe the preference of clinoptilolite exchange site(s) for K. Competition among precipitates for available elements in solution affects strongly the compositions of solid solutions, as well as the stability of individual phases in the mineral assemblage. Knowledge of general compositional trends of solid-solution phases with changes in temperature, ionic strength and other parameters is useful. However, realistic prediction of solid-solution compositions in response to changes in the environment can only be made if the competition for elements in the system, evidenced by mineral precipitation and dissolution, is taken into account.

Potential Impact of Fluid–Rock Interactions at Elevated Temperature

Several questions exist with reference to the chemistry of waters at Yucca Mountain and fluid–rock interactions accompanying increases in temperature. For example:

- Are Yucca Mountain waters in equilibrium with the subsurface mineralogy?
- Will mineralogy be significantly changed by heating of the near- and far-field environment?
- Will observed variations in repository water chemistry affect predictions of repository performance?

A series of EQ6 simulations were made simulating reaction between J–13 water and Topopah Spring tuff as a function of temperature to initiate a preliminary investigation of these and other issues.

Equilibrium between Yucca Mountain waters and subsurface mineralogy

Assuming that the precipitation of quartz is inhibited kinetically, the minerals cristobalite, dioctahedral smectite and stilbite are predicted by EQ3/6 to be the most likely phase assemblage in metastable equilibrium with J-13 water at 25 °C. The mineral assemblage should, in strict terms, be considered a metastable assemblage because of the presence of cristobalite rather than quartz. The zeolite clinoptilolite, rather than stilbite, coexists with cristobalite at Yucca Mountain. The stability of stilbite relative to other zeolites and its occurrences in nature should be studied further, as discussed earlier and in Appendix E. In the meantime, stilbite stability may be interpreted more generally as that of a zeolite of unknown identity, whose stability is enhanced by elevated SiO_2 activities.

The cristobalite-dioctahedral smectite-zeolite assemblage is consistent with the diagenetic mineralogy in diagenetic zones I and II at Yucca Mountain (see above). In general, the

activities of aqueous SiO_2 in Yucca Mountain waters are consistent with, and control, the secondary mineral assemblage with depth, as discussed previously. The activity diagram in Figure E.1 (Appendix E) shows that mordenite and clinoptilolite are in metastable equilibrium with solutions whose aqueous SiO_2 activity is controlled by amorphous silica or glass.

Although not calculated to be part of the stable phase assemblage, K-feldspar and clinoptilolite are close to equilibrium with J-13 water. K-feldspar and clinoptilolite are common phases in diagenetic zones I and II. The early appearance of authigenic K-feldspar is consistent with elevated SiO_2 concentrations in solution. In fact, it appears to be a reasonable way to produce early K-felaspar from dilute, near-neutral fluids.

Effect of temperature on interactions between J-13 water and Topopah Spring tuff

An increase in temperature may disrupt the state of metastable equilibrium between Yucca Mountain waters and the existing diagenetic mineralogy. The thermodynamic drive for fluids and rock to re-equilibrate may result in the formation of new stable phases and the destruction of previously-existing phases. Mineralogical changes may be deleterious to the physical and chemical properties of the tuff.

The interactions between Topopah Spring tuff and J-13 water caused by an increase in temperature from 25 to 90 °C in a closed system was simulated using EQ3/6. The paragenetic sequence in Figure 13 summarizes the evolution of the metastable mineral assemblage as a function of temperature. The assemblages are metastable because cristobalite was prohibited from converting to quartz in the simulation. The composition of J-13 water was taken from Delany (1985). The mineralogy of the tuff was approximated by cristobalite, alkali feldspar, plagioclase, Mg-beidellite and biotite (mineralogy of tuff core wafer from well USW G-1 in Delany, 1985). The minerals in the tuff were assumed to dissolve at rates proportional to their percentage by weight in the tuff. Tuff dissolved linearly with respect to temperature. At 90 °C, 10.68 grams of tuff had dissolved into 1 kilogram of J-13 water. This is equivalent to dissolution of 0.12 wt.% of the tuff given a porosity of 10%. Equilibrium was maintained between secondary phases and the solution at all times.

At 25 °C, the minerals predicted by EQ6 to be in metastable equilibrium with J-13 water are: cristobalite, stilbite and dioctahedral smectite (see above). The mineralogy evolves to a final assemblage of cristobalite, K-feldspar, clinoptilolite, dioctahedral smectite and muscovite as the temperature increases to 90 °C. Muscovite may serve as a proxy for an illitic component in a smectite/illite solid solution. The smectite/illite solid solution is not explicitly provided for in the geochemical model. The 90 °C mineral assemblage is significant in that it is similar to ambient mineralogy in diagenetic zone II at Yucca Mountain. This preliminary calculation suggests that increasing temperature will tend to favor the stability of minerals that are already abundant at Yucca Mountain.

The simulation results shown in Figure 13 were calculated assuming a given rate of dissolution of reactant minerals. However, the nature and sequence of secondary mineral assemblages resulting from tuff–water interactions near the waste package will depend on

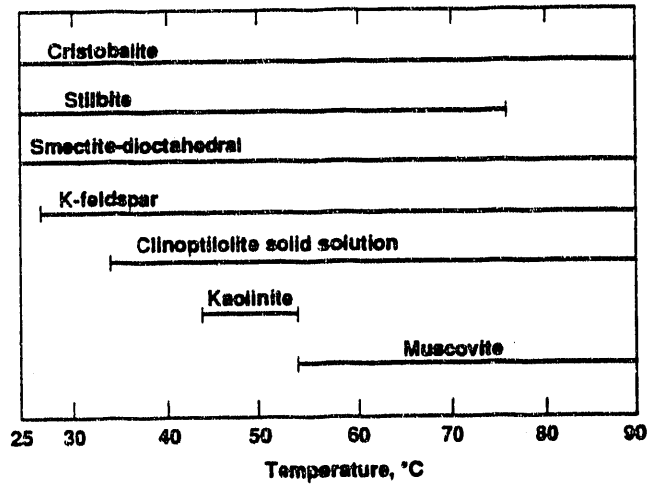

Figure 13. Predicted paragenetic sequence for reaction of Topopah Spring tuff with J-13 water from 25 to 90 °C (see text).

the balance between increases in temperature and the influx of chemical elements into solution through reactant mineral dissolution. Increasing the rates of dissolution in the previous simulation by one order of magnitude lowers temperatures at which the secondary minerals precipitate, but does not significantly affect their sequence. Decreasing rates by an order of magnitude expands or "stretches" the sequence of mineral precipitates, and results in an additional precipitate, celadonite.

Celadonite precipitates because of a temporary need to sequester released Mg prior to a significant increase in the mass of dioctahedral smectite, which sequesters Mg in the other simulations. The altered balance between temperature and dissolution rate does affect the mineral precipitates. However, the dissolution rate in many cases does not seem to significantly impact the general sequence and assemblages of mineral precipitates.

The ability to identify general mineralogical trends using only estimated dissolution rates rather than kinetic rate constants, simplifies modeling greatly. For some needs, it is sufficient to identify a general compositional trend, that is, the precipitation of a Mg–layer silicate, whether it be celadonite or a dioctahedral smectite, rather than a specific phase. More accurate models would, of course, use kinetic rate constants with a temperature and surface area dependence. The determination of mineral surface areas to be used in kinetic calculations is, however, problematic (White and Peterson, 1990). In view of the general consistency between calculational results made using estimated rates and kinetic rate constants, and the general complexity of kinetic calculations and the current uncertainty in their input parameters, it is convenient to use estimated dissolution rates in scoping calculations.

As discussed in the previous section, the transformation of the silica polymorphs appears to be a critical factor in the stability of zeolites. It was assumed in the previous calculations that cristobalite remained stable. If temperature, time or other forces change the identity of the silica polymorph and thus the activity of aqueous silica in solution, the mineralogical phase assemblage could change significantly. In a complete analysis of phase stability at Yucca Mountain under various waste disposal scenarios, it is necessary to account explicitly for the rates of transformation of the silica polymorphs as a function of temperature, time and other pertinent parameters.

In the previous simulation, the fugacities of O_2(gas) and CO_2(gas) were controlled by the fluid-tuff interaction. However, the fugacities of O_2(gas) and CO_2(gas) may be buffered by continuous contact with the atmosphere in the unsaturated zone at Yucca Mountain. Repeating the above simulation, but fixing the fugacities of O_2(gas) and CO_2(gas) at atmospheric values, yielded initial precipitates of calcite and talc in addition to cristobalite, stilbite and dioctahedral smectite. Talc is probably a proxy for a Mg–rich clay mineral. The final mineral assemblage consisted of cristobalite, K–feldspar, clinoptilolite, dioctahedral smectite and celadonite. Celadonite, a Mg–bearing mica, replaces muscovite in the final assemblage when the atmosphere buffers the CO_2(gas) fugacity.

The partial pressure of CO_2(g) in equilibrium with J–13 water ($10^{-2.5}$ bars) is actually higher than atmospheric, perhaps because of soil zone and biological activity. A reduction in CO_2(g) pressure from $10^{-2.5}$ bars to the atmospheric value of $10^{-3.5}$ bars causes an increase in solution pH. Hence, a different mineral assemblage is produced. However, it

remains that increased temperatures at Yucca Mountain will tend to produce mineralogic changes similar to those that the tuffs have already undergone through burial and time.

Effect of initial Eh and pH of J–13 water on mineralogic reactions

Measured pH and Eh (redox potential) vary somewhat from well to well and sample to sample in Yucca Mountain waters. Ranges in pH and Eh that have been measured in waters from Yucca Mountain wells are shaded in Figure 14 (Ogard and Kerrisk, 1984). The low Eh waters (minimum –0.191 V) were measured in so-called "thief" samples from well USW H-4. The "thief" samples were obtained by lowering a stainless steel container downhole and collecting a fluid sample at depth.

Even though the Eh of produced waters is usually measured, it is widely recognized that Eh is not a system variable. Redox pairs between aqueous species in natural waters tend to be in disequilibrium and have different redox potentials. The Eh measured by a given electrode may be a "mixed" potential that is not representative of any one couple. Problems also arise from the fact that electron transfer rates tend to be slow, and that natural waters tend to be poorly poised with respect to Eh (Scott and Morgan, 1990).

Most of the water samples from Yucca Mountain are "integral" samples, obtained by sampling at the wellhead after fluids have flowed to the surface. Various interactions can occur to change fluid chemistry as the fluids flow upward, especially if the flow is slow. All water-producing horizons are sampled, although flow-meters can be used to determine which zones are the dominant water-producers (e.g., Benson et al., 1983).

Water samples collected at the wellhead, whether they be thief or integral, are obtained from the saturated zone. However, the potential repository at Yucca Mountain is situated in the unsaturated zone. The chemical characteristics of water in the unsaturated zone are poorly known owing to difficulty in collection and analysis. pH and Eh may vary between the saturated and unsaturated zones.

Many other processes may alter fluid chemistry at Yucca Mountain. Fluid chemistry may be disturbed by reaction with engineered barrier system components (e.g., cements and metals) in the repository. The repository is expected to "dry-out" and then rehydrate; the chemical composition of waters returning to the waste package may vary significantly from the compositions of present-day saturated zone waters. Given the uncertainties in our knowledge of the Eh and pH of repository waters, to what extent will potential variations in the pH and Eh of water impact future water–rock reactions?

To determine the extent to which variations in Eh and pH may influence fluid–rock reactions, computer simulations were conducted in which Topopah Spring tuff was reacted with J–13 water at 90°C. Four simulations were made in which the initial J-13 water was assumed to be characterized by four different Eh–pH states. The combinations of pH and Eh, represented by the four corners of the trapezoid in Figure 14, were: 7 and –0.20 volts; 10 and –0.20 volts; 7 and 0.80 volts; 10 and 0.63 volts. The range in pH and the minimum in Eh were selected from measured values outlined in Figure 14. The maximum Eh values were chosen to represent fugacities of oxygen in equilibrium with the atmosphere at pH values of 7 and 10.

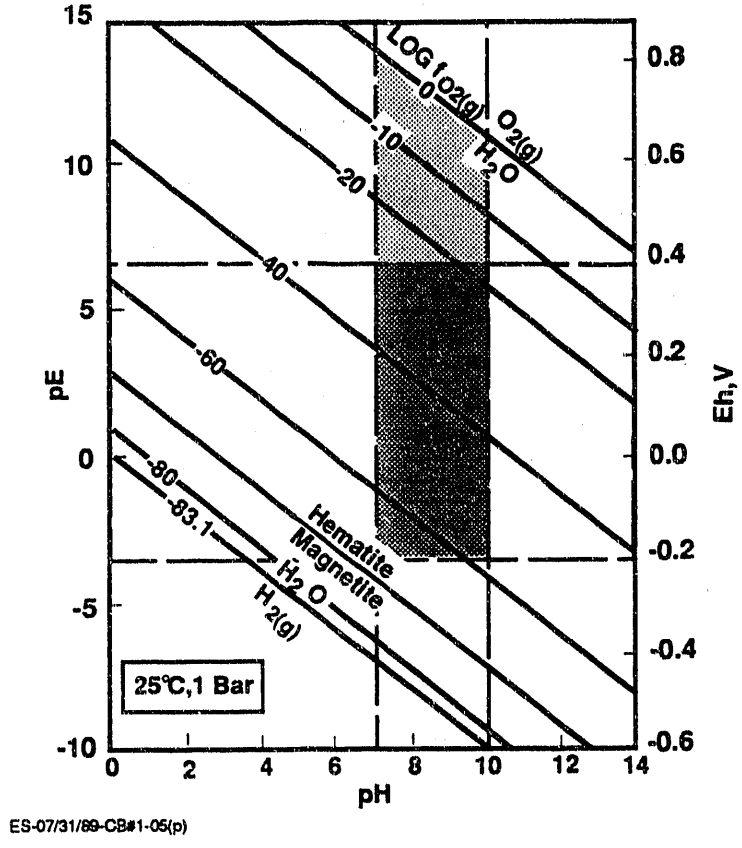

Figure 14. Ranges in Eh and pH (dark shaded area) measured in Yucca Mountain waters from the saturated zone. Data from Ogard and Kerrisk (1984). Light shaded area shows upper limits of Eh and pH used in simulations shown in Figure 15 (see text).

The simulations were conducted with the same starting materials and, except for Eh, pH and temperature, under the same conditions as the simulation discussed in the previous section and summarized in Figure 12. Simulation results differ because of the isothermal conditions, and because of the differences in Eh and pH during the simulations.

The paragenetic sequence in Figure 15a summarizes the solid dissolution/precipitation events occurring during fluid–rock interaction when the initial pH of J-13 water equalled 7, but the initial Eh varied from 0.80 to –0.20 volts. Results are presented as a function of the grams of dissolved rock per kilogram of water. The mineral paragenesis shown in the middle of Figure 15a is common to both simulations; the mineral stabilities at the top and bottom of the central paragenetic sequence are unique to each simulation. It can be seen that the calculated paragenetic sequences are quite similar, and differ only because of the impact of Eh on the precipitation of Fe–bearing phases. At a starting Eh of 0.80 volts, an Fe–rich dioctahedral smectite precipitated initially. At an initial Eh of –0.2 volts, pyrite precipitated initially, but then co–precipitated with dioctahedral smectite.

The two simulations with an initial pH of 10 but different Eh values produced identical paragenetic sequences, shown in Figure 15b. Eh had no effect on the mineralogical changes with elevated temperature when the starting pH equalled 10. An Fe–rich garnet precipitated initially in both runs to sequester Fe.

In all four EQ6 simulations, similar final diagenetic sequences were attained after dissolution of about 10 grams of tuff into a kilogram of water. Differences among the final assemblages included the appearance of celadonitic layer silicate rather than muscovite when the initial pH was high, and pyrite in one of the low Eh runs. The trend to a similar mineral assemblage reflects the gradual transition of the systems from fluid–dominated to rock–dominated. The x–axis of Figures 15 a and b can be interpreted as a measure of the rock:fluid ratio. These preliminary calculations suggest that the impact of variations of pore water pH and Eh on fluid-rock interactions will be greatest during the early stages of reaction. The impact will be minimized as the rock and fluid continue to react and the rock:fluid ratio increases.

Future work should be directed to examining consequences of variations in water chemistry in addition to pH and Eh on mineral reactions. Variations in water chemistry owing to interaction with man-made materials, including the waste package and engineered barrier system, over a range of temperature could be considered in the evaluation of potential scenarios of waste disposal. The calculations are also useful in evaluating conceptual models of mineral and fluid evolution at Yucca Mountain. Recently-available kinetic data on rates of mineral dissolution and precipitation can be incorporated into the computer models to attempt to calculate rates of mineral transformations with temperature. Problems that must be addressed in the future include predicting the stability of zeolites with greater confidence, with special reference to stilbite.

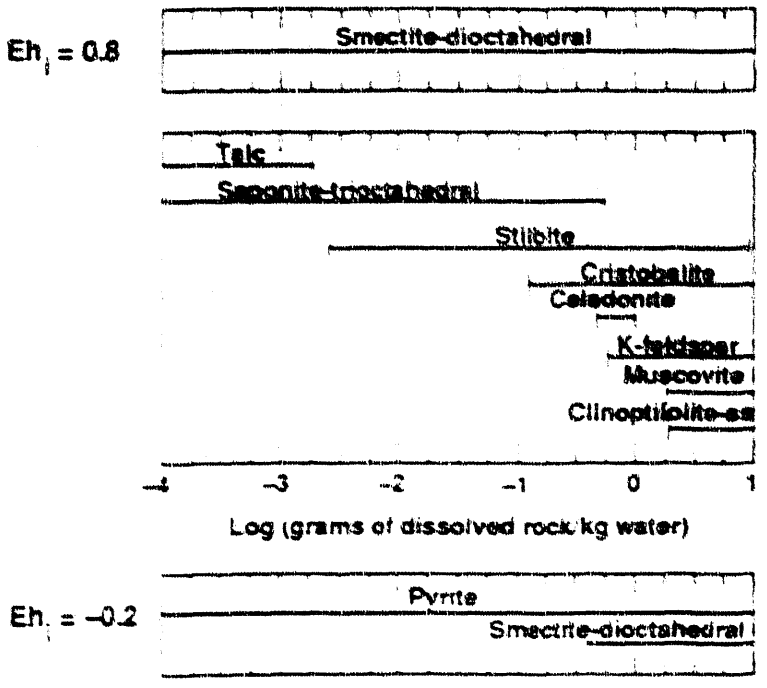

(a)

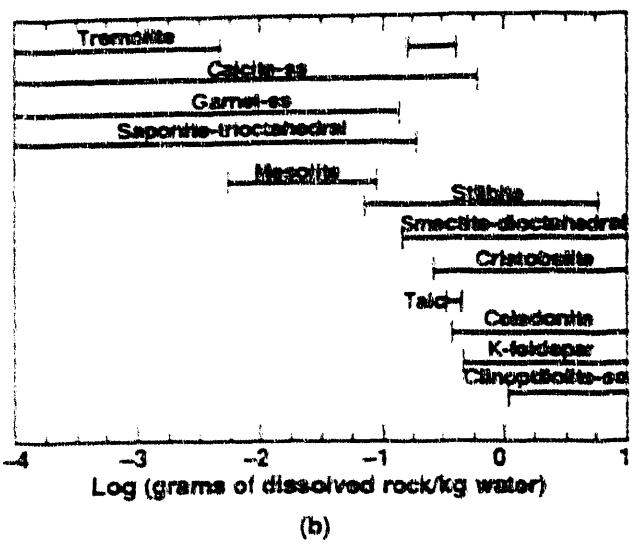

(b)

Figure 15. Predicted paragenetic sequences for reaction of Topopah Spring tuff with J–13 water at 90 °C assuming initial J–13 waters with a) pH = 7 and Eh of 0.8 and –0.2 volts; and b) pH = 10 and Eh of 0.63 and –0.2 volts (see text).

References

Aagaard, P., and Helgeson, H.C., 1983, Activity/composition relations among silicates and aqueous solutions: II. Chemical and thermodynamic consequences of ideal mixing of atoms on homological sites in montmorillonites, illites, and mixed-layer clays: *Clays and Clay Minerals*, v. 31, p. 207–217. (NNA.891006.0210)

Ames, Jr., L.L., 1964a, Some zeolite equilibria with alkali metal cations: *Amer. Mineralogist*, v. 49, p. 127–145. (NNA.890918.0520)

Ames, Jr., L.L., 1964b, Some zeolite equilibria with alkaline earth metal cations: *Amer. Mineralogist*, v. 49, p. 1099–1110. (NNA.890918.0521)

Barrer, R.M., 1978, Cation-exchange equilibria in zeolites and feldspathoids: in Sand, L.B. and Mumpton, F.A., eds., *Natural Zeolites*, p. 385–396, Pergamon Press. (NNA.920401.0106)

Barrer, R.M., Papadopoulos, R., and Rees, L.V.C, 1967, Exchange of sodium in clinoptilolite by organic cations: *J. Inorg. Nucl. Chem.*, v. 29, p. 2047–2063. (Readily available)

Benson, L.V. and McKinley, P.W., 1985, Chemical composition of ground water in the Yucca Mountain area, Nevada, 1971–84: U.S. Geological Survey Open-file Report 85–484, 10 p. (NNA.900207.0281)

Benson, L.V., Robison, J.H., Blankennagel, R.K. and Ogard, A.E., 1983, Chemical composition of ground water and the locations of permeable zones in the Yucca Mountain area, Nevada: U.S. Geological Survey Open-file Report 83–854, 19 p. (NNA.900207.0281)

Bish, D.L., 1988, Effects of composition on the dehydration behavior of clinoptilolite and heulandite: in *Occurrence, Properties and Utilization of Natural Zeolites*, Kallo, D. and Sherry, H.S., eds., Akademiai Kiado Pub., Budapest. (NNA.890525.0001)

Bish, D.L., 1984, Effects of exchangeable cation composition on the thermal expansion/contraction of clinoptilolite: *Clays and Clay Minerals*, v. 32, p. 444–452. (Readily available)

Bish, D.L. and Chipera, S.J., 1989, Revised mineralogic summary of Yucca Mountain, Nevada: Los Alamos National Laboratory, Los Alamos, NM, LA-11497, 68 p. (NNA.891019.0029)

Bourcier, W.L., 1985, Improvements in the solid solution modeling capabilities of the EQ3/6 geochemical code: Lawrence Livermore National Laboratory, Livermore, CA, UCID-20587. (NNA.920529.0029)

Brouwer, E., Baeyens, B., Maes, A., and Cremers, A., 1983, Cesium and rubidium ion equilibria in illite clay: *J. Phys. Chem.*, v. 87, p. 1213–1219. (Readily available)

Broxton, D.E., Bish, D.L. and Warren, R.G., 1987, Distribution and chemistry of diagenetic minerals at Yucca Mountain, Nye County, Nevada: *Clays and Clay Minerals*, v. 35, p. 89–110. (NNA.890222.0053)

Broxton, D.E., Warren, R.G., Hagan, R.C. and Luedemann, G., 1986, Chemistry of diagenetically-altered tuffs at a potential nuclear waste repository, Yucca Mountain, Nye County, Nevada: Los Alamos National Laboratory, Los Alamos, NM, LA-10802, 160 p. (NNA.890327.0036)

Chipera, S.J., and Bish, D.L., 1989, Quantitative X-ray diffraction analyses of samples used for sorption studies by the Isotope and Nuclear Chemistry Division, Los Alamos National Laboratory: Los Alamos National Laboratory, Los Alamos, NM, LA-11669-MS, 19 p. (NNA.890414.0062)

Delany, J.M., 1985, Reaction of Topopah Spring tuff with J-13 water: A geochemical modeling approach using the EQ3/6 reaction path code: Lawrence Livermore National Laboratory, Livermore, CA, UCRL-53631, 46 p. (NNA.871111.0114)

Delany, J.M. and Lundeen, S.R., 1991, The LLNL thermochemical data base-- Revised data and file format for the EQ3/6 package: Lawrence Livermore National Laboratory, Livermore, CA, UCID-21658, 59 p. (NNA.910619.0022)

Duffy, C.J., 1984, Hydrothermal chemistry: in *Research and development related to the Nevada Nuclear Waste Storage investigations*, Los Alamos National Laboratory, Los Alamos, NM, LA-10032, p. 12-19. (Readily available)

Fletcher, P. and Sposito, G., 1989, The chemical modelling of clay/electrolyte interactions for montmorillonite: *Clay Minerals* v. 24, p. 375-391. (Readily available)

Flotow, H.E. and Osborne, D.W. 1974, The heat capacity of dicesium monoxide from 5 to 350 K and the Gibbs energy of formation to 763 K: *J. Chem. Thermod.*, v. 6, p. 135-140. (Readily available)

Frysinger, G.R., 1962, Caesium-sodium ion exchange on clinoptilolite: *Nature*, v. 194, p. 351-353. (Readily available)

Fuentes, H.R., Polzer, W.L., Gruber, J., Lauctes, B., and Essington, E.H., 1987, Preliminary report on sorption modeling: Los Alamos National Laboratory, Los Alamos, NM, LA-10952. (NNA.900206.0221)

Gast, R.G., 1972, Alkali metal cation exchange on Chambers montmorillonite: *Soil Sci. Soc. Amer. Proc.*, v. 36, p. 14-19. (Readily available)

Glassley, W., 1986, Reference waste package environment report: Lawrence Livermore National Laboratory, Livermore, CA, UCRL-53726. (NNA.920506.0035)

Helgeson, H.C., and Aagaard, P., 1985, Activity/composition relations among silicates and aqueous solutions I. Thermodynamics of intrasite mixing and substitutional order/disorder in minerals: *Amer. J. Sci.*, v. 285, p. 769-844. (Readily available)

Helgeson, H.C., Delany, J.M., Nesbitt, H.W., and Bird, D.K., 1978, Summary and critique of the thermodynamic properties of rock-forming minerals: *Amer. J. Sci.*, v. 278-A, p. 1-229. (Readily available)

Hemingway, B.S, and Robie, R.A., 1977, Enthalpies of formation of low albite ($NaAlSi_3O_8$), gibbsite ($Al(OH)_3$), and $NaAlO_2$: Revised values for $\Delta H^\circ_{f,298}$ and $\Delta G^\circ_{f,298}$ of some aluminosilicate minerals: *J. Res. U.S. Geol. Survey,* v. 5, p. 413–429. (Readily available)

Howell, D.A., Johnson, G.K., Tasker, I.R., O'Hare, P.A.G. and Wise, W.S., 1990, Thermodynamic properties of the zeolite stilbite: *Zeolites,* v. 10, p. 525–531. (NNA.920529.0015)

Howery, D.G., and Thomas, H.C., 1965, Ion exchange on the mineral clinoptilolite: *J. Phys. Chem.*, v. 69, p. 531–537. (Readily available)

Hulbert, M., 1987, Sodium, calcium, and ammonium exchange on clinoptilolite from Fort LaClede deposit, Sweetwater County, Wyoming: *Clays and Clay Minerals*, v. 35, p. 458–462. (Readily available)

Iijima, A., 1988, Diagenetic transformations of minerals as exemplified by zeolites and silica minerals – A Japanese view. Part I. Zeolitic diagenesis: in *Diagenesis, II, Developments in Sedimentology 43,* G. V. Chilingarian and K. H. Wolf, eds., Elsevier, New York, p. 147–188. (NNA.920506.0039)

Johnson, G.K., Flotow, H.E., and O'Hare, P.A.G., 1983, Thermodynamic studies of zeolites: natrolite, mesolite and scolecite: *Amer. Miner.*, v. 68, p. 1134–1145. (NNA.920529.0016)

Johnson, G.K., Flotow, H.E., and O'Hare, P.A.G., 1985, Thermodynamic studies of zeolites: heulandite: *Amer. Miner.*, v. 70, p. 1065–1071. (NNA.920529.0017)

Johnson, G.K., Flotow, H.E., O'Hare, P.A.G. and Wise, W.S., 1982, Thermodynamic studies of zeolites: analcime and dehydrated analcime: *Amer. Miner.*, v. 67, p. 736–748. (NNA.920529.0018)

Johnson, G.K., Tasker, I.R., Flotow, H.E., O'Hare, P.A.G., and Wise, W.S., 1992, Thermodynamic studies of mordenite, dehydrated mordenite, and gibbsite: *Amer. Miner.*, v. 77, p. 85–93. (NNA.920529.0019)

Johnson, G.K., Tasker, I.R., Jurgens, R. and O'Hare, P.A.G., 1991, Thermodynamic studies of zeolites: clinoptilolite: *J. Chem. Therm.*, v. 23, p. 475–484. (NNA.920529.0020)

Kelley, K.K. 1960, *Contributions to the Data on Theoretical Metallurgy, xiii. High-temperature Heat Content, Heat Capacity, and Entropy Data for the Elements and Inorganic Compounds,* U.S. Bureau of Mines Bulletin 584, p. 21. (NNA.920529.0021)

Kerrisk, J.F., 1983, Reaction-path calculations of groundwater chemistry and mineral formation at Rainier Mesa, Nevada: Los Alamos National Laboratory, Los Alamos, NM, LA–9912, 41 p. (NNA.900125.0104)

Knauss, K.G., 1987, Zeolitization of glassy Topopah Spring tuff under hydrothermal conditions: Mat. Res. Soc. Symp., Proc. v. 84, p. 737–745. (NNA.920302.0050)

Knauss, K.G. and Peifer, D.W., 1986, Reaction of vitric Topopah Spring tuff and J-13 ground water under hydrothermal conditions using Dickson-type, gold-bag rocking autoclaves: Lawrence Livermore National Laboratory, Livermore, CA, UCRL-53795, 39 p. (NNA.891102.0117)

Kubaschewski, O., and Alcock, C.B. 1979, *Metallurgical Thermochemistry*, 5th ed., Pergamon Press, p. 353. (NNA.920529.0022)

Laudelot, H., Van Bladel, R., and Robeyns, J., 1971, The effect of water activity on ion exchange selectivity in clays: *Soil Science*, v. 111, p. 211-213. (Readily available)

Levy, S.S., 1984, Petrology of samples from drill holes USW H-3, H-4, and H-5, Yucca Mountain, Nevada: Los Alamos National Laboratory, Los Alamos, NM, LA-9706, 77 p. (NNA.870519.0048)

Ogard, A.E. and J.F. Kerrisk, 1984, Groundwater chemistry along flow paths between a proposed repository site and the accessible environment: Los Alamos National Laboratory, Los Alamos, NM, LA-10188, 48 p. (NNA.890907.0118)

Rimstidt, J.D., Newcomb, W.D., Shettel, D.L., Jr., 1989, A vertical thermal gradient experiment to simulate conditions in vapor dominated geothermal systems, epithermal gold deposits, and high level radioactive repositories in unsaturated media: in *Water-Rock Interaction WRI-6*, Proceedings of the 6th Intl. Symp., Malvern, U.K., D.L. Miles. ed., A.A. Balkema, Brookfield, p 585-588. (NNA.920319.0007)

Robie, R.A., Hemingway, B.S., and Fisher, J.F., 1978, Thermodynamic properties of minerals and related substances at 298.15 K and 1 Bar (10^5 Pascals) pressure and at higher temperatures: U.S. Geological Survey Bulletin 1452, 456 p. (NNA.900702.0002)

Scott, M.J. and Morgan, J.J., 1990, Energetics and conservative properties of redox systems: in *Chemical Modeling of Aqueous Systems II*, D.C. Melchior and R.L. Bassett, eds., American Chemical Society Symposium Series Volume 416, Washington, D.C., p. 368-378. (Readily available)

Smyth, J.R. and Bish, D.L. 1988, *Crystal Structures and Cation Sites of the Rock-forming Minerals*: Allen and Unwin, Boston, MA., p. 245. (NNA.920529.0023)

Smyth, J.R., Spaid, A.T., and Bish, D.L., 1990, Crystal structures of a natural and a Cs-exchanged clinoptilolite: *Amer. Miner.*, v. 75, p. 522-528. (Readily available)

Sposito, G., 1981, *Thermodynamics of Soil Solutions*: Oxford University Press, New York, NY. (NNA.900416.0124)

Thomas, K.W., 1987, Summary of sorption measurements performed with Yucca Mountain, Nevada, tuff samples and water from well J-13: Los Alamos National Laboratory, Los Alamos, NM, LA-10960-MS. (NNA.890602.0026)

Viani, B.E. and Bruton, C.J., 1992, Modeling ion exchange in clinoptilolite using the EQ3/6 geochemical modeling code: Lawrence Livermore National Laboratory, Livermore, CA, UCRL-JC-109952. (NNA.920805.001)

Wagman, D.D., Evans, W.H., Parker, V.B., Schumm, R.H., Halow, I., Bailey, S.M., Churney, K.L., and Nuttall, R.L., 1982, *The NBS Tables of Chemical Thermodynamic Properties, Selected Values for Inorganic and C1 and C2 Organic Substances in SI Units*: J. Phys. Chem. Reference Data, v. 11, Suppl. 2, pp. 276 and 282. (NNA.920529.0024)

White, A.F. and Peterson, M.L., 1990, Role of reactive-surface-area characterization in geochemical kinetic models: in *Chemical Modeling of Aqueous Systems II*, Melchior, D.C. and Bassett, R.L., eds., American Chemical Society Symposium Series Volume 416, Washington, D.C., p. 461–475. (NNA.920529.0025)

Wolery, T.J., 1983, EQ3NR: A Computer Program for Geochemical Aqueous Speciation–Solubility Calculations, User's Guide and Documentation: Lawrence Livermore National Laboratory, Livermore, CA, UCRL–53414. (HQS.880517.2912)

Wolery, T.J., Jackson, K.J., Bourcier, W.L., Bruton, C.J., Viani, B.E., Knauss, K.G. and Delany, J.M., 1990, The EQ3/6 software package for geochemical modeling: Current status: in *Chemical Modeling in Aqueous Systems II*, D.C. Melchior and R.L. Bassett, eds., American Chemical Society Symposium Series Volume 416, p. 104–116. (Readily available)

Wood, B.J. and Fraser, D.G., 1977, Multicompent solids and fluids: in *Elementary Thermodynamics for Geologists*: Oxford University Press, Oxford, UK, Chapter 3, p. 81–126. (NNA.920506.0033)

Appendix A.

Derivation of Modified Ideal Site-Mixing Solid-solution Model

The modified ideal site-mixing model can be derived from an ideal site–mixing model by assuming that cations and vacancies do not mix independently of one another on a crystallographic site. First it is shown that the activity of a solid–solution *component* can be described in terms of the *ideal mixing* of atoms and *vacancies* occupying structurally defined sites. Using a single–site solid solution of clinoptilolite as an example, it is pointed out that ideal mixing of *atoms* on a site does not insure that the mixing of solid–solution *components* is ideal. Next, it is shown that modifying the ideal site–mixing model by coupling the exchange of vacancies to multivalent cations, yields a solid-solution model in which the mixing of *components is ideal* and numerically equivalent to the Gapon exchange model. The Vanselow exchange model is then analyzed using a site-mixing description. Finally, the ideal and modified ideal site-mixing models are compared.

Ideal mixing of ions and vacancies on a site – The activity of a component end-member in a solid solution can be described in terms of the occupancy of atoms and vacancies on the crystallographic sites in the solution. For ideal mixing of atoms on a *single type* of site, the activity of the *k*th component is (Aagaard and Helgeson, 1983; Helgeson and Aagaard, 1985)

$$a_k = \prod_j \left[\frac{x_j}{x_{j,k}} \right]^{\nu_{j,k}} , \qquad \text{(A.1)}$$

where x_j is the mole fraction of the *j*th cation or vacancy occupying the site in *the solid solution*, $x_{j,k}$ is the mole fraction of the *j*th cation occupying the site in the *k*th *component*, and $\nu_{j,k}$ is the stoichiometric number of the *j*th cation on that site in one mole of the *k*th *component*.

Ideal mixing of ions and vacancies applied to a single–site clinoptilolite – For a clinoptilolite solid solution, the activity of an end-member component with monovalent cation *M* expressed according to Eq. (A.1) is given by

$$a_{mono,M^+} = (x_{M^+})^N , \qquad \text{(A.2)}$$

where x_{M+} is the mole fraction of monovalent cation *M* on the exchange site in the clinoptilolite solid solution, and *N* represents the negative charge for one mole of the solid-solution as used in Eq. (2). For end-member components with divalent cations, this relationship becomes

$$a_{di,M^{++}} = \left(\frac{x_{M^{++}}}{0.5}\right)^{N/2}\left(\frac{x_{vac}}{0.5}\right)^{N/2} , \qquad (A.3)$$

where x_{M++} is the mole fraction of divalent cation M on the exchange site in the clinoptilolite solid solution, and x_{vac} is the mole fraction of the *vacancy* on the site. The x_{M+}, x_{M++}, and x_{va} mole fractions are based on the sum of *cations and vacancies* occupying the site.

The relationship between the mole fraction of a *cation or vacancy on the site* and the mole fraction of the *component in the solid solution* that contributes that cation is

$$x_{M^{+}} = X_{mono,M^{+}} \qquad (A.4)$$

for monovalent cations,

$$x_{M^{++}} = \frac{X_{di,M^{++}}}{2} \qquad (A.5)$$

for divalent cations, and

$$x_{vac} = \frac{\sum_i X_{M_i^{++}}}{2} \qquad (A.6)$$

for vacancies, where $X_{mono,M^{+}}$ and $X_{di,M^{++}}$ are the mole fractions of mono and divalent cation bearing components respectively, and $\sum_i X_{M_i^{++}}$ is the sum of mole fractions of all divalent components in the solid solution.

Substituting the right sides of Eqs.(A.4) – (A.6) into Eqs. (A.2) and (A.3) yields the following activity-composition relationships

$$a_{mono,M^{+}} = (X_{mono,M^{+}})^{N} \qquad (A.7)$$

and

$$a_{di,M^{++}} = (X_{di,M^{++}})^{N/2}\left[\sum_i X_{M_i^{++}}\right]^{N/2} . \qquad (A.8)$$

Ideal mixing of atoms on sites* vs. *ideal mixing of end-member components – As pointed out by Helgeson and Aagaard (1985), ideal mixing of atoms on sites does not necessarily im-

ply that mixing of *end-member components* is ideal. For example, a solid solution in which an atom or vacancy on a site can be contributed by *more than one component* would be non-ideal with respect to the mixing of end-member components, even if it behaves ideally with respect to mixing of atoms on crystallographic sites. Thus, if compositional variation on the exchange site of clinoptilolite were described using ideal site-mixing, the mixing of clinoptilolite *end-member components* would be non-ideal because *vacancies* can be contributed from *any of the end-member components with multivalent cations in the exchange site*. The activity of end-members with multivalent cations would be described by Eq. (A.8). As a consequence, binary heterovalent exchange isotherms, predicted using an ideal-site mixing model, are strongly affected by the concentration of a second multivalent cation on the exchange site (Figure 1).

Modifying the ideal site-mixing relationship: Preventing vacancies from mixing independently of multivalent cations – As far as we are aware, there are no reported data for exchange in clinoptilolites involving more than two cations (ternary or greater exchange) that could be used to test the implications of the ideal site-mixing model. Therefore, it was *assumed* that the end-member components in clinoptilolite mix ideally according to Eq. (2):

$$a_k = X_k^N \quad . \tag{2}$$

The above relationship follows from the ideal site-mixing model only if the entities that mix on the site are *coupled cation-vacancies*. We assume that the "atomic" entity that mixes on the site is $M_{1/m}V_{(1-1/m)}$, where M is a cation of valence m and V is a vacancy. For all end-members, regardless of the valence of the exchange cation, there are N moles of coupled cation-vacancies per mole of component (which is equal to *N equivalents of M).* When the coupled cation-vacancy is substituted in the site-mixing relationship (Eq. (A.1)), Eq. (2) is obtained (Table A.1). This activity-composition relationship is numerically identical to the Gapon cation-exchange convention (Appendix D) and insures that the activity of any one component *is solely dependent* on the concentration of that component in the solid solution. It is the simplest relationship that can be used to describe mixing on a single exchange site.

If it is assumed that the exchange of multivalent cations is coupled to that of vacancies, but that the "atomic" entity that mixes on the site can be identified with the *moles* of the *cation* occupying the site, the resulting activity-composition relationship is numerically identical to the Vanselow exchange convention (Appendix D). In this instance, the entity that mixes on the site is defined as $MV_{(m-1)}$ (Table A.1). Because the mole fraction of a coupled cation-vacancy in a solid solution (x_j) is a function of the mole fractions (X_k) and valences (m_k) of all other components and cations in the solid solution (Table A.1), this relationship, like the ideal site-mixing relationship, implies that the activity of any one component is dependent on the concentration of other components of the solid-solution (i.e., the mixing of *components* is non-ideal) (Figure 1).

Table A.1. Site-mixing parameters for coupled cation-vacancies describing Gapon and Vanselow exchange models.

Model	Coupled (1) Cation-Vacancy (cv_L)	Site-Mixing Parameters (2) $\nu_{j=cv_L,k=L}$	$x_{j=cv_L,k=L}$	$x_{j=cv_L}$	Component Activity $a_{k=L}$
Gapon	$cv_L \equiv M_{1/m_L}V_{(1-1/m_L)}$	N	1	X_L (3)	X_L^N
Vanselow	$cv_L \equiv MV_{(m_L-1)}$	N/m_L	1	$\frac{X_L/m_L}{\sum_k (X_k/m_k)}$	$\left[\frac{X_L/m_L}{\sum_k (X_k/m_k)}\right]^{N/m_L}$

(1) Formula of coupled cation-vacancy, cv_L, where M represents a cation with valence m_L occupying the exchange site of end-member L, and V represents a vacancy.

(2) Parameters have the same meaning as used in Eq. (A.1) except that $\nu_{j,k}$ and $x_{j,k}$ refer to the stoichiometric number and mole fraction of the jth *cation-vacancy* in the kth end-member, respectively, and x_j is the mole fraction of the cation-vacancy in the solid solution. Note that for $k=L$, $\nu_{j,k}$ and $x_{j,k}$ are 0 for all j not equal to cv_L.

(3) X_L represents the mole fraction of end-member $k=L$ in the solid solution.

The *modified site-mixing model* differs from the ideal site-mixing model in several respects: 1) the solid solution is ideal; that is, the mixing between any two components is unaffected by the presence of any other component; 2) for multisite solid-solution models, such as that being developed for smectites, mixing on the exchange sites is independent of mixing on structural sites; and, 3) the form of the mixing relationship is consistent with a commonly used ion-exchange formalism, the Gapon convention, which assumes that the activity of an exchange cation is equal to its *equivalent* fraction (App. D; Sposito, 1981).

Appendix B.

Implementation in EQ3/6 – Solid-Solution Model

To simulate compositional variation of solid solutions, it is necessary to be able to predict the composition of the solid solution that is most supersaturated or least undersaturated with respect to the aqueous phase. This is done by finding the *composition of the solid solution that maximizes the saturation index function, SI* (Bourcier, 1985). For a phase of fixed composition, SI is defined as

$$SI = \log\left[\frac{Q}{K}\right] , \tag{B.1}$$

where Q is the ion activity product and K is the equilibrium constant for the mineral dissolution reaction. For a solid solution with n components, SI is defined as

$$SI = \sum_{k=1}^{n} X_k \log\left[\frac{Q_k}{K_k a_k}\right] , \tag{B.2}$$

where Q_k and K_k are the activity product and equilibrium constant for the hydrolysis reaction of the kth component, and a_k is the activity of the kth component in the solid solution. For a solid solution in which the activity of the component follows the modified ideal site-mixing relationship defined by Eq. (2), SI is

$$SI = \sum_{k=1}^{n} X_k \log\left[\frac{Q_k}{K_k X_k^N}\right] , \tag{B.3}$$

Following the method of Bourcier (1985), Eq. (B.3) is differentiated with respect to X_k, equated to zero, combined with Eq. (B.3), and an equation obtained to calculate the X_k's that maximize SI,

$$X_k = \left[\frac{Q_k/K_k}{\sum_{k=1}^{n} Q_k/K_k}\right]^{1/N} , \tag{B.4}$$

where N is the number of energetically equivalent positions on the site. Modifications to the routines in EQ3/6 that calculate SI and X_k were made to implement this model.

Appendix C.

Estimation of Entropy and Heat Capacity Power Function Coefficients

Third-law molar entropies and heat capacity power function coefficients for end-member components of the hydrated and dehydrated clinoptilolite studied by Johnson et al. (1991) were estimated using the algorithms presented by Helgeson et al. (1978). In the method of Helgeson et al. (1978), the properties of an unknown phase are estimated by referencing its properties to structurally similar phases, whose thermodynamic properties are known, via a solid–solid reference reaction. Reference exchange reactions were written between the end-member of interest and the mixed-composition clinoptilolite studied by Johnson et al. (1991), using oxides to balance the reaction stoichiometry. An example of a reference reaction for the Na–clinoptilolite end-member is

$$\mathrm{Na_{3.467}}-\text{clinoptilolite}\cdot x\mathrm{H_2O} = \mathrm{Na_{0.954}K_{0.543}Ca_{0.761}Mg_{0.124}Ba_{0.062}Sr_{0.036}Mn_{0.002}}-\text{clinoptilolite}\cdot y\mathrm{H_2O}$$

$$+\ 1.257\ \mathrm{Na_2O} - 0.272\ \mathrm{K_2O} - 0.761\ \mathrm{CaO} - \mathrm{O}.124\ \mathrm{MgO}$$

$$- 0.062\ \mathrm{BaO} - 0.036\ \mathrm{SrO} - 0.002\ \mathrm{MnO} + (x-y)\mathrm{H_2O}\ . \quad \text{(C.1)}$$

Estimation of entropy – The third law molar entropy, S°, was calculated according to

$$S_k^\circ = \frac{\sum_i \nu_i S_i^\circ \left[\sum_i \nu_i V_i^\circ + V_k^\circ\right]}{2\sum_i \nu_i V_i^\circ}\ , \quad \text{(C.2)}$$

where S_k° and V_k° refer to the entropy and molar volume of the kth end-member of the solid solution on the left-hand side of the reference reaction, and S_i°, V_i°, and ν_i refer to the entropy, molar volume and reaction coefficient of the ith phase on the right-hand side of the reaction.

Estimation of heat capacity power function coefficients – The heat capacity power function coefficients were calculated by assuming the heat capacity change of the reference reaction is zero; that is,

$$\sum_i \nu_i C_{p\,i} - C_{p\,k} = 0\ . \quad \text{(C.3)}$$

where $C_{p\,i}$ is the heat capacity of the ith phase on the right-hand side of the reference reaction and $C_{p\,k}$ is the heat capacity of the kth end-member of the solid solution.

The power function used to describe the heat capacity of an end-member component of clinoptilolite is

$$C_{p\,k} = a_k + b_k T^{-2} + c_k T + d_k T^2 \qquad \text{(C.4)}$$

for which the coefficients were calculated according to

$$\begin{aligned} a_k &= \sum_i \nu_i a_i \ , \\ b_k &= \sum_i \nu_i b_i \ , \\ c_k &= \sum_i \nu_i c_i \quad \text{and} \\ d_k &= \sum_i \nu_i d_i \ , \end{aligned} \qquad \text{(C.5)}$$

where a_k, b_k, ck, and d_k are the coefficients of the heat capacity power function for the kth end-member component, and a_i, b_i, c_i, and d_i are the coefficients for the phases on the right side of the reference reaction.

Heat capacity polynomials and $S°$ for natural clinoptilolite and dehydrated clinoptilolite were used as reported by Johnson et al. (1991). For the hydrated clinoptilolite, it was assumed that *all* end-members contained the same number of waters of hydration as reported by Johnson et al. (1991). Molar volumes for the end-members and the reference clinoptilolite were assumed to be equal to one another and assigned a value of 632.05 (Smyth and Bish, 1988) and 544.7 cm^3 for hydrated and dehydrated clinoptilolite, respectively. The latter value was computed assuming that the molar volume of zeolitic water is 8 cm^3 (Helgeson et al., 1978). Data for the oxides (except Cs_2O, BaO, and SrO) were taken from Helgeson et al. (1978). The $S°$ and $V°$ data for Cs_2O were taken from Robie et al. (1978), and the polynomial function coefficients were determined by fitting the heat capacity measurements of Flotow and Osborne (1974). For BaO and SrO, the $S°$ data were taken from Wagman et al. (1982), the $V°$ data from Robie et al. (1978), and the heat capacity polynomial coefficients from Kelley (1960) and Kubaschewski and Alcock (1979), respectively.

Appendix D.

Implementation in EQ3/6 – Cation-Exchange Models

Cation-exchange models were implemented in a manner to allow simulation of multiple exchangers, exchangers with multiple types of exchange sites, exchangers that are not in overall equilibrium with the aqueous solution, and exchangers for which solubility data are not available. These requirements were met by treating exchangers as if they were *aqueous species*. Implementation of the models required the following:

1. Exchanger "ligands" were added to the GEMBOCHS (version data0.R19) basis species set. Aqueous exchanger/cation complexes, with stoichiometries conforming to the Gapon and Vanselow models, were defined in data0 by appropriate dissociation reactions using the exchanger basis species.
2. The calculation of activity coefficients in EQ3/6 (version 3245.R141 of EQLIB) for the aqueous exchanger/cation complexes was modified to conform to Gapon and Vanselow conventions.
3. The input files and associated subroutines (versions 3245.R116 and 3245.R106 of EQ3 and EQ6, respectively) were modified to accept cation-exchange data in a convenient format.

Additions to the thermodynamic data base: Dissociation reactions – In order to model cation exchange by considering the exchanger to be an aqueous "ligand", it was necessary to consider the ligand to be a new "element". Each exchanger was added to the data base as an element and also included in the EQ3/6 basis species set (Wolery, 1983) as a univalent anion. Three such elements were defined, allowing up to three different exchangers, or a single exchanger with three independent sites, to be modeled in a given simulation.

Aqueous/exchanger complexes, having stoichiometries conforming to the Gapon and Vanselow components, were defined in the data base by appropriate *dissociation reactions* written in terms of the exchanger ligand basis species and the exchange cation. Any two dissociation reactions may be used to define a cation exchange reaction; that is, each dissociation reaction can be considered a half-exchange reaction. Twenty eight dissociation reactions have been defined for each exchange model.

Vanselow model dissociation reactions – The dissociation reactions and corresponding mass action equations that define the cation/exchanger complexes for Na and Ca according to the Vanselow model are

$$\mathrm{Na}\text{–}Z = \mathrm{Na}^+ + Z^- \qquad K_1 = \frac{a_{\mathrm{Na}^+}\, a_{Z^-}}{a_{\mathrm{Na}\text{–}Z}} \qquad \text{(D.1)}$$

and

$$\frac{1}{2}\ \mathrm{Ca\text{-}Z_2} = \frac{1}{2}\ \mathrm{Ca^{++}} + \mathrm{Z^-} \qquad K_2 = \frac{a_{\mathrm{Ca^{++}}}^{1/2}\ a_{Z^-}}{a_{\mathrm{Ca\text{-}Z_2}}^{1/2}}\ , \tag{D.2}$$

where $a_{\mathrm{Na\text{-}Z}}$, $a_{\mathrm{Ca\text{-}Z_2}}$, and a_{Z^-} represent the activities of the Na-exchanger *aqueous complex*, Ca-exchanger *aqueous complex*, and uncomplexed *exchanger ligand*, respectively. By adding reaction (D.1) to the reverse of (D.2), the reaction for the exchange of Na by Ca is obtained (i.e., Eq. (5) written for one equivalent of exchange).

Gapon model dissociation reactions – The *monovalent* exchanger/cation complexes are the same for both Vanselow and Gapon models (i.e., the Na exchange complex is defined by (D.1)). The dissociation reaction and mass action relationship corresponding to the Gapon model for the Ca exchange complex are

$$\mathrm{Ca_{1/2}\text{-}Z} = 1/2\ \mathrm{Ca^{++}} + \mathrm{Z^-} \qquad K_3 = \frac{a_{\mathrm{Ca^{++}}}^{1/2}\ a_{Z^-}}{a_{\mathrm{Ca_{1/2}\text{-}Z}}}\ . \tag{D.3}$$

The dissociation constants K_1, K_2 and K_3 are set to 10^{-20} in the data base to prevent the ligand, Z^-, from contributing appreciably to the ionic strength of the solution, and to insure that the exchange sites are "fully occupied". When the activities of the *aqueous exchanger complexes* conform to the definition of activity for the *exchange components* for ideal exchange (i.e., according to Eqs. (7) and (11)), then $K_1/K_2 = K_V$ and $K_1/K_3 = K_G$.

Vanselow model $$a_{M\text{-}Z_m} \equiv X_{M\text{-}Z_m} = x_M \tag{7}$$

Gapon model $$a_{M_{1/m}\text{-}Z} \equiv X_{M_{1/m}\text{-}Z} = E_M \tag{11}$$

Modification of activity coefficient routine in EQ3/6 – To insure conformance with the definitions of exchanger component activities, modifications were made to the EQ3/6 routine that calculates aqueous species activity coefficients.

Vanselow model – To conform to Eq. (7), the activity of a given *Vanselow aqueous complex* must equal the *mole fraction* of the cation in that complex based on the sum of all the cations complexed by that exchanger ligand; that is,

$$a_{M_k\text{-}Z_{m_k}} = \frac{c_{M_k\text{-}Z_{m_k}}}{\sum_k^n c_{M_k\text{-}Z_{m_k}}}\ , \tag{D.4}$$

where $a_{M_k\text{-}Z_{m_k}}$ is the activity of the aqueous complex formed between Z^- and cation M_k, and $c_{M_k\text{-}Z_{m_k}}$ is the *molal concentration* of this complex. The equality defined by Eq. (D.4)

is insured by equating the activity coefficients for Vanselow aqueous exchanger complexes to the term $1/\sum_{k}^{n} c_{M_k\text{-}Z_{m_k}}$. The activity coefficient for the uncomplexed ligand is set to unity.

Gapon model – To conform to Eq. (11), the activity of a given *Gapon aqueous complex* must equal the *equivalent fraction* of the cation in that complex based on the sum of all the cations complexed by that exchanger ligand; that is,

$$a_{M_{1/m_k}\text{-}Z} = \frac{c_{M_{1/m_k}\text{-}Z}}{T_Z} \quad , \tag{D.5}$$

where T_Z, the total equivalents of exchanger per kg of water, is set on input and remains constant during a simulation and $c_{M_{1/m_k}\text{-}Z}$, the molal concentration of the Gapon aqueous complex, is numerically equal to the equivalents per kg of cation M_k. Eq. (D.5) is adhered to by equating the activity coefficient for Gapon aqueous exchanger complexes to the term $1/T_Z$.

Cation-exchange option input – Modifications were made to the EQ3NR input file and the routine that reads it so that: (1) exchange data could be specified in a convenient format on input without the user having to add to or modify data0; (2) it is not necessary for the user to recalculate input quantities for the cationic species specified in the simulation; and (3) log K's for the *dissociation reactions* are automatically adjusted to be consistent with the log K's of the *exchange reactions* that are input. To use the cation exchanger option in EQ3/6, the *free energies per equivalent of exchanger* of the binary exchange reactions (or their appropriate log K's) are specified in the input file for each exchanger and/or site named by the user. The quantity of exchanger or site, in equivalents per kg of water, and its initial cationic composition (in mole or equivalent percent) are also specified. The total quantity of a cation in the simulation, the sum of that input as an aqueous species and that input via the exchanger, is automatically calculated. The log K's of the appropriate aqueous complex dissociation reactions are adjusted to insure consistency with the ideal binary exchange reaction log K's as defined by Eqs. (8) and (12); thus, considering Na/Ca exchange, $K_1/K_2 = K_V$ and $K_1/K_3 = K_G$.

Appendix E.

Thermochemical Data for Clinoptilolite

Johnson and co-workers determined calorimetrically the thermodynamic properties of a variety of zeolites, including clinoptilolite (Howell et al., 1990; Johnson et al., 1982, 1983, 1985, 1991, 1992). However, Johnson et al. (1992) suggest that the thermodynamic properties of zeolites should be referenced to the heat of fusion for silicalite rather than α-quartz. They also used their recently determined enthalpy data for gibbsite (ΔH_f° = −1294.9 ± 1.2 kJ/mol) in the thermochemical cycle for the derivation of ΔH_f°, rather than the value of Hemingway and Robie (1977) (ΔH_f° = −1293.13 ± 1.19 kJ/mol) that they had used previously. The latter value is used in the EQ3/6 data base.

Results of geochemical modeling simulations suggest that zeolites appear to be unreasonably stable with respect to other aluminosilicates when their thermodynamic properties are referenced to silicalite. Predictions of natural assemblages appear to be more reasonable when zeolite data are referenced to α-quartz instead. Most of the data in the EQ3/6 data base are also referenced directly or indirectly to the thermodynamic properties of α-quartz rather than silicalite. We have, therefore, recalculated the thermodynamic data reported by Howell et al. (1990) and Johnson et al. (1991, 1992) for clinoptilolite and other zeolites to maintain consistency with the thermodynamic data for α-quartz and gibbsite in the EQ3/6 data base.

Tables E.1 and E.2 list the thermodynamic properties and heat capacity power functions for clinoptilolite and other zeolites in the EQ3/6 data base that were revised from data in Howell et al. (1990) and Johnson et al. (1991, 1992). The data for clinoptilolite were used to derive the standard state properties of the homoionic end-members of the clinoptilolite solid solution, as discussed in the text.

The activity diagram shown in Figure E.1 was constructed using the thermodynamic data for zeolites listed in Table E.1 to illustrate stability relationships among the zeolites and other aluminosilicates as a function of fluid composition. The activity diagram was constructed for the compositional system Na–K–Ca–Al–Si–H_2O at 25 °C assuming the existence of pure end–member components of clinoptilolite. The dashed lines represent saturation lines for the silica polymorphs. If the thermodynamic data for the zeolites listed in Table E.1 had been referenced to silicalite, the zeolites, especially the SiO_2–rich clinoptilolite end–members and mordenite, would have dominated the entire activity diagram, which contradicts natural occurrences of aluminosilicate minerals.

Table E.1. Thermodynamic properties of selected zeolites in EQ3/6 data base data0.com.R7.(1)

Zeolite(2)	$\Delta H^{\circ}_{f,298}$ kJ/mol	$C_{p,298}$ J/mol-K	$S^{\circ}_{298} - S^{\circ}_{0}$ (3) J/mol-K	$\Delta G^{\circ}_{f,298}$ kJ/mol
Analcime	−3296.9 ± 3.3	211.53 ± 0.21	226.75 ± 0.23	−3077.2 ± 3.3
Dehydrated Analcime	−2970.2 ± 3.5	163.59 ± 0.16	171.71 ± 0.17	−2803.7 ± 3.5
Natrolite	−5718.6 ± 5.0	359.23 ± 0.72	359.73 ± 0.72	−5316.6 ± 5.0
Mesolite	−5947.1 ± 5.4	371. ± 2	363. ± 2	−5513.2 ± 5.4
Scolecite	−6049.0 ± 5.0	382.81 ± 0.77	367.42 ± 0.73	−5597.9 ± 5.0
Heulandite	−10594.6 ± 10.2	781.03 ± 0.78	767.18 ± 0.77	−9779.1 ± 10.2
Stilbite	−11005.7 ± 6.6	808.73 ± 1.62	805.54 ± 1.61	−10114.1 ± 6.6
Mordenite	−6736.7 ± 4.5	484.33 ± 0.97	486.54 ± 0.97	−6228.1 ± 4.5
Dehydrated Mordenite	−5642.3 ± 4.6	295.76 ± 0.59	299.1 ± 0.6	−5319.2 ± 4.6
Clinoptilolite	−20587.8 ± 13.5	1537.44	1483.06	−19021.2
Dehydrated Clinoptilolite	−17210.2 ± 13.4	882.92	893.31	−16227.3

(1) Original data from Johnson et al. (1991, 1992) and Howell et al. (1990) modified to correct the base reactions for SiO_2 from silicalite to α-quartz and for $Al(OH)_3$ from Johnson et al.'s (1992) value for $\Delta H_f^{\circ}(Al(OH)_3)$ to that in the EQ3/6 data base (see text).

(2) Formula units:

Analcime	$Na_{0.96}Al_{0.96}Si_{2.04}O_6 \cdot H_2O$
Natrolite	$Na_2Al_2Si_3O_{10} \cdot 2H_2O$
Mesolite	$(Na_{0.676}Ca_{0.657})Al_{1.990}Si_{3.01}O_{10} \cdot 2.647H_2O$
Scolecite	$CaAl_2Si_3O_{10} \cdot 3H_2O$
Heulandite	$(Ba_{0.065}Sr_{0.175}Ca_{0.585}K_{0.132}Na_{0.383})Al_{2.165}Si_{6.835}O_{18} \cdot 6.00H_2O$
Stilbite	$(Ca_{1.019}Na_{0.136}K_{0.006})Al_{2.180}Si_{6.820}O_{18} \cdot 7.33H_2O$
Mordenite	$(Ca_{0.289}Na_{0.361})Al_{0.940}Si_{5.060}O_{12} \cdot 3.468H_2O$
Clinoptilolite	$(Sr_{0.036}Mg_{0.124}Ca_{0.761}Mn_{0.002}Ba_{0.062}K_{0.543}Na_{0.954})Al_{3.45}Fe_{0.017}Si_{14.533}O_{36} \cdot 10.922H_2O$

(3) Because the entropy at 0 K is unknown, the difference between the entropy at 298 and that at 0 K is tabulated.

The stabilities of the Na- and Ca-clinoptilolite end-members and mordenite are favored by high $SiO_{2(aq)}$ activity, which is consistent with natural occurrences of these zeolites and with experimental results (Knauss, 1987; Knauss and Peifer, 1986). A broad stability field

for stilbite exists for a wide range of $SiO_{2(aq)}$ activities. Provision for solid solution between the Na–clinoptilolite and Ca–clinoptilolite end–members would move the boundary between the clinoptilolites and stilbite, grossular and kaolinite to $SiO_{2(aq)}$ activities closer to equilibrium with cristobalite. Stilbite would still occupy a significant chemical space, nonetheless.

Stilbite occurs in basic to silicic volcanic rocks as a result of hydrothermal alteration and contact metamorphism (Iijima, 1988). Iijima (1988) states that stilbite and other calcic zeolites such as mordenite, heulandite, laumontite, yugawaralite and wairakite are characteristic of hydrothermal alteration in a high geothermal gradient. Rimstidt, Newcomb and Shettel (1989) observed stilbite precipitating as a secondary mineral during laboratory-induced boiling/condensation cycles in volcanic tuffs. It remains to be seen whether the predicted stability of stilbite is in agreement with its natural occurrences, and whether its appearance relative to other phases is controlled by kinetics and/or other phenomena, rather than equilibrium.

Table E.2. Heat capacity power function coefficients and temperature limits of applicability for selected zeolites in EQ3/6 data base data0.com.R7. (1,2)

	a	b	c	d	e	C_p limit K
Analcime	237.6303	——	-0.474284	1.66566×10^{-3}	-1.23602×10^{-6}	625
Dehydrated Analcime	110.799	-1.58298×10^{6}	0.27172	-1.17153×10^{-3}	——	1000
Natrolite	301.957	-4.897565×10^{6}	0.37688	——	——	660
Mesolite(3)	190.7774	-1.632521×10^{6}	0.6793	——	——	470
Scolecite	135.1876	——	0.83053	——	——	470
Heulandite	745.55	-1.410835×10^{7}	0.65133	——	——	475
Stilbite	442.961	——	0.617338	3.60856×10^{-3}	-5.2472×10^{-6}	500
Mordenite	528.09	-8.196591×10^{6}	0.16249	——	——	500
Dehydrated Mordenite	305.95	-7.704565×10^{6}	0.30447	-1.60833×10^{-4}	——	900
Clinoptilolite	50.155	——	6.3645	-4.6156×10^{-3}	——	500
Dehydrated Clinoptilolite	-478.07	——	6.9104	-9.0309×10^{-3}	3.9018×10^{-6}	700

(1) C_p (J/mol-K) = $a + bT^{-2} + cT + dT^2 + eT^3$
(2) Data from Howell et al. (1990) and Johnson et al. (1982, 1983, 1985, 1991, 1992). See Table E.1 for mineral formulas.
(3) The heat capacity power function for mesolite was estimated by assuming that $\Delta Cp_{rxn} = 0$ for the reaction 0.657 scolecite + 0.338 natrolite = mesolite.

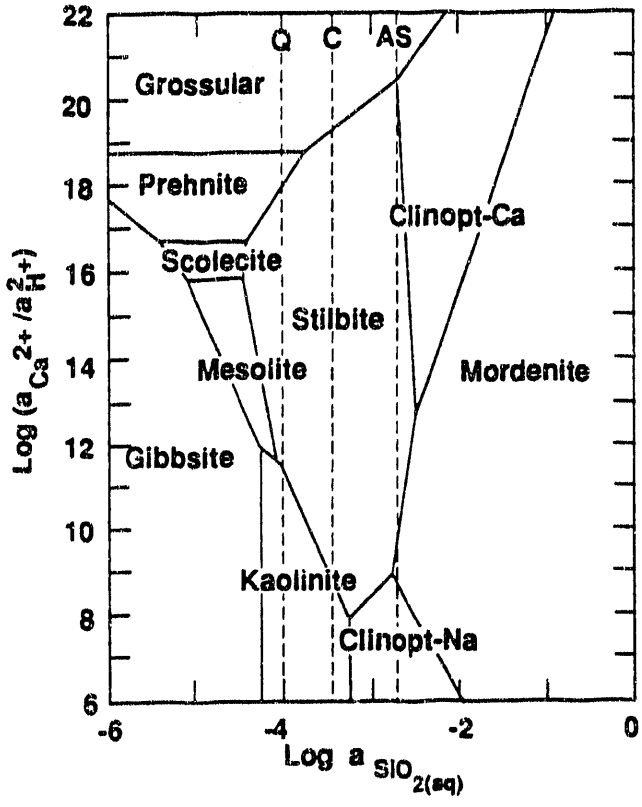

Figure E.1. Activity diagram for the system Na–K–Ca–Al–Si–H_2O at 25 °C depicting mineral stability as a function of the logarithm of the activity (a) of aqueous silica in solution (SiO_2(aq)) and the logarithm of the ratio of the activity of the Ca^{2+} ion to the square of the activity of H^+ ion in solution. Vertical lines are saturation boundaries for the silica polymorphs: Q = quartz; C = cristobalite; AS = amorphous silica. Data from thermodynamic data base data0.com.R7.

END

DATE
FILMED
12/21/92